Water budget, performance of evapotranspiration formulations, and their impact on hydrological modeling of a small boreal peatland-dominated watershed

Pierre-Erik Isabelle[a,*], Daniel F. Nadeau[b], Alain N. Rousseau[c], François Anctil[d]

a: Department of Civil and Water Engineering, Université Laval, 1065 avenue de la Médecine, Québec, QC, Canada. pierre-erik.isabelle.1@ulaval.ca

b: Department of Civil and Water Engineering, Université Laval, 1065 avenue de la Médecine, Québec, QC, Canada. daniel.nadeau@gci.ulaval.ca

c: Institut national de la recherche scientifique – Centre Eau Terre Environnement, 490 rue de la Couronne, Québec, QC, Canada. alain.rousseau@ete.inrs.ca

d: Department of Civil and Water Engineering, Université Laval, 1065 avenue de la Médecine, Québec, QC, Canada. francois.anctil@gci.ulaval.ca

* Corresponding author: Pierre-Erik Isabelle, Department of Civil and Water Engineering, Université Laval, 1065 avenue de la Médecine, Québec, QC, Canada. 418-955-1496. pierre-erik.isabelle.1@ulaval.ca

Abstract

Peatlands occupy around 13% of the land cover of Canada, and thus play a key role in the water balance at high latitudes. They are well known for having substantial water loss due to evapotranspiration. Since measurements of evapotranspiration are scarce over these environments, hydrologists generally rely on models of varying complexity to evaluate these water exchanges in the global watershed balance. This study quantifies the water budget of a small boreal peatland-dominated watershed. We assess the performance of three evapotranspiration models in comparison with *in situ* observations and the impact of using these models in the hydrological modeling of the watershed. The study site (~1-km^2) is located in the Eastern James Bay lowlands, Québec, Canada. During summer 2012, an eddy flux tower measured evapotranspiration continuously, while a trapezoidal flume monitored streamflow at the watershed outlet. We estimated evapotranspiration with a combinational model (Penman), a radiation-based model (Priestley-Taylor), and a temperature-based model (Hydro-Québec), and performed the hydrological modeling of the watershed with HYDROTEL, a physically-based semi-distributed model. Our results show that the Penman and Priestley-Taylor models reproduce the observations with the highest precision, while a substantial drop in performance occurs with the Hydro-Québec model. However, these discrepancies did not appear to reduce the hydrological model efficiency, at least from what can be concluded from a 3-month modeling period. HYDROTEL appears sensitive to evapotranspiration inputs, but calibration of model parameters can compensate for the differences. These findings still need to be confirmed with longer modeling periods.

KEYWORDS: Peatland hydrology; Eddy covariance; Evapotranspiration model; Watershed modeling; Sensitivity analysis.

Introduction

Wetlands are estimated to cover between 5 and 6 million km^2, equivalent to roughly 4% of the emerged Earth surface (Matthews and Fung, 1987; Aselmann and Crutzen, 1989). In Canada, wetlands cover 14% of the land, of which 90% are peatlands (NWWG, 1997; Price et al., 2005). Canadian peatlands are mostly found in the boreal and subarctic zones (Tarnocai et al., 2005). They are especially dominant in the James Bay and Hudson Bay lowlands, one of the largest peatland area in the world (Gorham, 1991), where peatland is the sole land surface type in many locations (e.g. Glaser et al., 2005; Leclair et al., 2015).

This type of environment is known to transform rapidly under climate changes and fluctuations (Bidgham et al., 2008; Dise, 2009; Runkle et al., 2014), even more so at high latitudes (IPCC, 2013). As northern regions are more and more subject to human development, accurately quantifying the water budget of these environments becomes critical for the perennity of these sensitive ecosystems. With such a high land surface occurrence and sensitivity to climate non-stationarity, boreal peatlands have to be modeled thoroughly by climatologists and hydrologists interested in water pathways across boreal regions.

Considerable efforts must be put into quantifying the actual evapotranspiration (ET_a), as it is the only inherent link between the water and energy budgets, and therefore between hydrology and climatology during snow-free periods. In boreal peatlands, ET_a occupies a fairly variable fraction of the water budget; on an annual basis, cumulative ET_a can amount to between 40% and 85% of the annual precipitation (Verry, 1988; Brümmer et al., 2012). This percentage increases significantly when one considers only the snow-free period, with some examples for which nearly all of the precipitation (P) returns to the atmosphere as ET_a (Isabelle, 2014; Runkle et al., 2014). Wu et al. (2010) have shown that ET_a / P also varies greatly between a wet growing season (~62%) and a dry one (~140%). In the James Bay lowlands, ET_a losses are the most important control on freshwater runoff to the saline bay during the summer (Isabelle, 2014). As a result, ET_a has to be properly estimated.

However, the precision (related to random error, i.e. variance of the error) and accuracy (related to systematic error, i.e. mean error) of ET_a estimations are often sacrificed at the expense of simpler and faster modeling strategies. This practice raises two questions: (i) which type of model best reproduces ET_a of a boreal peatland? ; and (ii) does a lesser quality in modeled ET_a systematically lead to a poorer agreement between simulated and observed watershed streamflow?

A great number of studies have assessed the performance of various ET_a modeling strategies for boreal peatlands, most of them have been reviewed by Drexler et al. (2004). The general consensus is that increasing the complexity of a model leads to a better representation of the ET_a. These authors, however, point out that these more complex models rely on site-specific calibration and the accuracy of the measurements.

Meanwhile, several studies have focused on the impacts of the potential evapotranspiration precision (ET_p; ET when water supply is unlimited at the surface) on hydrological modeling. Andréassian et al. (2004) did a comprehensive review on this subject. Table 1 presents methodological details from the studies listed by Andréassian et al. (2004), but including one more recent paper (Oudin et al., 2005) and this study. The main takeaway is that, most of the time, the precision of input ET_p

(and hence of modeled ET_a) does not largely influence the quality of the hydrological modeling. This conclusion seems to be valid whether the temporal (Fowler, 2002; Oudin et al., 2005) and spatial (Andréassian et al., 2004) precisions of ET_p are improved or the precision of the ET_p model is increased (Andersson, 1992; Nandakumar and Mein, 1997; Joukainen, 2000; Kokkonen and Jakeman, 2001; Oudin et al., 2005). Most authors agree that the calibration of the model can compensate for varying ET_p precision. Nevertheless, ET_p models have been shown to be a great source of variability in hydrological predictions under changing climate conditions (Donohue et al., 2010; Seiller and Anctil, 2014). Moreover, some studies found that using a simple temperature-based ET_p model can lead to serious offsets in hydrological predictions, when calibration is virtually impossible (Lofgren et al., 2011; Hoerling et al., 2012).

The aforementioned analyses mostly focused on large watersheds and multiple years of data. However, one could think that on reduced temporal and spatial scales, the precision of the ET_a would have a larger influence on the outcome of the hydrological model. Indeed, as smaller scales imply that water flow amplitudes are diminished as a whole, slight variations of one term could substantially affect the water budget, a consideration relevant under operational conditions. An advantage of studying a smaller watershed, even for a short period, is the possibility to use ET_a measurements as input to the hydrological model.

Such measurements can be obtained by applying the eddy covariance method, deemed one of the most reliable and accurate approach to measure ET_a (Itier and Brunet, 1996). With an optimal experimental setup, the measured ET_a is then representative of the whole small-scale watershed while accounting for the high ET_a

diurnal variability. None of the aforementioned studies have compared the performance of a hydrological model using sophisticated ET_a measurements or common, but less-precise ET_p models. Furthermore, to the best of our knowledge, this type of analysis has not previously been done on boreal peatland-dominated watersheds. In addition, understanding the impacts of ET_a on the hydrological modeling of peatlands is critical around James Bay for the ecosystems preservation and the hydroelectric exploitation of rivers.

The research conveyed in this paper quantifies the water budget of a small peatland-dominated watershed. We have two specific objectives: (i) to compare several ET_p models with *in situ* observations on a James Bay lowland peatland; and (ii) to estimate the impact of using ET_p models in lieu of ET_a measurements as inputs to an hydrological model in that type of environment.

Materials

Study site: Necopastic peatland

The Necopastic peatland watershed drains 97 ha, of which 63% is occupied by a peatland (Clerc, 2009), while the rest of the watershed is boreal forest (20%) and rocky outcrops (17%). The peatland is mostly ombrotrophic, meaning that it receives all its water and nutrients from precipitation rather than from upstream runoff and groundwater. Named after the nearby Necopastic River, a tributary to La Grande River, the Necopastic peatland is located in the James Bay lowlands, northern Québec, Canada (53°40'28"N; 78°10'14" W, elevation: 105 m ASL). Figure 1a shows a satellite image of the watershed (Google Earth, 2017) along with the location of the instruments and other landmarks, with the location in Canada as an inset. Figure 1b presents a topographical map of the watershed, which has a slope of 0.013 m m^{-1}. The initial watershed boundary was identified by Clerc (2009) using interpretation of airborne image and confirmed on the field with GPS points. As determining watershed extent is especially delicate in low relief environments, the boundaries were further refined by an extended analysis of the digital elevation model of the area.

The vegetative cover was thoroughly surveyed by Clerc (2009) and further described by Nadeau et al. (2013). The peatland portion of the watershed is mostly covered with *Sphagnum* mosses, lichens and shrubs, with some scattered spruce, larch, and jack pine trees, 1 to 4 m tall, covering a 1.6 thick peat layer. This peatland is surrounded by a black spruce forest with 6 to 8 m trees. The climate is subarctic, with a strong influence from the nearby James Bay. A mean annual temperature of -2.4 °C and mean annual precipitation of 697 mm (35% as snow) was observed over the period 1977-2011 (Nadeau et al., 2013).

Experimental setup

During summer 2012, the Necopastic peatland watershed was instrumented to measure most components of the energy and water budgets. The main feature of the experimental setup was a 6-m flux tower (see Figure 1c) using the eddy covariance method to measure sensible and latent heat fluxes (H and LE, respectively) and evapotranspiration ($ET_{a,EC}$). It consisted of a three-dimensional sonic anemometer (CSAT-3, Campbell Scientific, USA) equipped with a fine-wire thermocouple and an open-path CO_2/H_2O gas analyzer (LI-7500, LI-COR Biosciences, USA).

Turbulent fluxes were computed using EddyPro®, version 5.0 (LI-COR Biosciences, USA), an open-source software designed to process eddy covariance data. The performed data processing is described in Nadeau et al. (2013) and Isabelle et al. (2015). Uncertainties are associated with the use of the eddy covariance method.

Random sampling errors (Finkelstein and Sims, 2002), underestimation of turbulent fluxes with an unclosed energy balance (Foken, 2008), and spatial extrapolation of local measurements to the whole watershed are the most critical. We elaborate on these issues in the *Discussion*.

Net radiation R_n was monitored with a 4-component radiometer (CNR1, Kipp and Zonen, The Netherlands), while soil heat flux G was measured with soil heat flux plates (HFT3, Campbell Scientific, USA). Note that since heat flux plates have been known to perform poorly in *Sphagnum* mosses (Rouse, 1984; Rouse et al., 1987; Halliwell and Rouse, 1987; Petrone et al., 2004), their measurements were verified successfully with the calorimetric method, that is: the sum of the heat energy intake over several layers of a vertical soil temperature profile (Halliwell and Rouse, 1987; Ochsner et al., 2007).

Several other components of the water budget were measured, aside from the ET_a. This budget may be expressed as an equality between incoming (left-hand side) and outgoing and change in stored (right-hand side) water:

$$P = ET_a + Q + S + \text{Residual} \tag{1}$$

where Q is river discharge [mm], and S, change in groundwater storage [mm] over the monitored time interval. Precipitation P [mm] inputs were measured with a tipping-bucket rain gauge in the direct vicinity of the flux tower (CS700H, Campbell Scientific, USA) and cumulated every 30 min.

The water table was monitored with two wells located within a 100-m distance of the flux tower (see Figure 1a,b) and equipped with level sensors (Level Loggers, Solinst, USA). Soil water content in the unsaturated zone was measured with two soil water content reflectometers (CS616, Campbell Scientific, USA). The instruments were installed horizontally at 3 cm and 15 cm depth. As the factory calibration is problematic in peat soils, the instruments were used to compute the apparent dielectric constant of the sampled soil (Hansson and Lundin, 2006). With those values, volumetric water content was obtained with the peat-specific empirical function of Kellner and Lundin (2001).

This setup was used to compute the saturated and unsaturated portion of *S*. The saturated part was taken as the water table height difference between two time steps, multiplied by the soil porosity at the water table depth. The latter was obtained at the 3 cm and 15 cm depth as the maximum volumetric water content at saturation, with values of 0.92 and 0.86, respectively. The porosity was assumed constant at 0.86 below 15 cm, and a linear interpolation was made between the two known values from 15 cm to 3 cm deep. Water storage in the unsaturated zone was computed taking the difference in water content between two time steps multiplied by the depth of the unsaturated zone. *S* is then the sum of the unsaturated and saturated parts.

The streamflow at the watershed outlet *Q* was monitored with a 12-in trapezoidal flume (SRCRC, Accura-Flo™, USA) (see Figure 1d). The residual is taken as a water outflow or storage; meaning that a positive value implies that water entering the watershed exceeds that coming out or stored. Obviously, this term accounts for measurement uncertainties, as well as possible other terms that do not appear in Equation 1 such as lateral groundwater flow. However, we note that the incoming part of the latter is usually negligible for ombrotrophic peatlands (Aselmann and Crutzen, 1989). Outgoing lateral groundwater flow could be important, especially in the southwest part of the bog (see Figure 1a) where a channel may form between the ponds present.

Every measured variable was averaged (or summed for P) over a 30-min timescale and stored using a datalogger (CR-5000 for $ET_{a,EC}$ fluxes, CR-3000 for the rest, Campbell Scientific, USA). P and $ET_{a,EC}$ were next summed on hourly and daily time steps for hydrological modeling. The study period extended from 24 June to 27 September 2012. Maintaining such a remote site is very challenging, and as result the experimental period is rather short from a hydrological standpoint. Still, it does not prevent the dataset from being unique and appropriate to answer the proposed scientific questions. The study focuses on summer conditions because it is the period where ET_a has the largest influence on the water budget, especially at these high latitudes.

Methods

Comparison of modeled ET_a with observations

ET_p models

We tested a hierarchy of models of contrasting complexities and development philosophies to estimate ET_p: Penman (1948), Priestley and Taylor (1972) and a temperature-based empirical equation commonly used in hydrological engineering applications in northern Québec (St-Hilaire et al., 2003; Minville et al., 2008, 2009), hereby referenced to as the Hydro-Québec model. As there is a great number of temperature-based ET_p equations with relatively similar efficiencies (Oudin et al., 2005, Seiller and Anctil, 2016), we chose the Hydro-Québec model because it is hypothetically the best-calibrated for the study site region.

The most complex of these models is the Penman model, originally developed to describe evaporation from an open-water surface. The model, also considered applicable over saturated land surfaces, combines energy-balance and mass-transfer approaches to include contributions from the available energy ($R_n - G$) and unsaturated atmosphere to ET_p. The Penman model can be written as follows:

$$ET_{p,PM} = \frac{1}{L_v}\left[\frac{\Delta}{\Delta+\gamma}\left(R_n - G\right) + \frac{\gamma}{\Delta+\gamma}E_A\right] \tag{2}$$

where $ET_{p,PM}$ [kg m^{-2} s^{-1}] is the water vapor flux; L_v [J kg^{-1}], the latent heat of vaporization of water; Δ [Pa K^{-1}], the slope of saturation vapor pressure versus temperature curve; γ [Pa K^{-1}], the psychrometric constant; R_n [W m^{-2}], the net radiation; G [W m^{-2}], the ground heat flux; and E_A [W m^{-2}], the drying power of the air, defined by Katul and Parlange (1992) as:

$$E_A = \frac{L_v \kappa^2 \bar{\rho}\bar{u}\left(\bar{q}_* - \bar{q}\right)}{\ln\left(\frac{z_v - d_0}{z_{0v}}\right)\ln\left(\frac{z_m - d_0}{z_{0m}}\right)} \tag{3}$$

where κ is the von Kármán constant (= 0.4); $\bar{\rho}$ [kg m^{-3}], the humid air density; $\bar{u}$ [m s^{-1}], the mean wind velocity measured at height z_m [m]; $\bar{q}$ [kg kg^{-1}], the mean specific humidity measured at height z_v [m]; $\bar{q}_* = \bar{q}_*\left(T_a\right)$ [kg kg^{-1}], the specific humidity of the air at saturation; and the overbars are time averages over a 30-min period; z_{0m} and z_{0v} [m], the roughness lengths for momentum and humidity, respectively; d_0 [m], the zero-plane displacement height. d_0, z_{0m} and z_{0v} are estimated with the mean vegetation height at the site (h_v = 0.5 m) as (2/3)h_v, 0.1h_v and 0.01h_v, respectively (Brutsaert, 1982; 2005).

The Priestley-Taylor model is an empirical simplification of the Penman model valid for wet surfaces under conditions of limited advection. This radiation-based model is often used as the description of equilibrium ET, meaning ET coming from a saturated surface to a saturated atmosphere. It is described as:

$$ET_{p,PT} = \frac{1}{L_v}\left[\frac{\Delta}{\Delta+\gamma}\left(R_n - G\right)\right] \quad (4)$$

where $ET_{p,PT}$ [kg m^{-2} s^{-1}] is also a water vapor flux. Usually, the formulation of $ET_{p,PT}$ includes a scale factor α to convert equilibrium ET to ET_p. We also included an α scale factor to the model, but to convert equilibrium ET to ET_a (more details in the next section).

Hydro-Québec is the government-owned public power utility responsible for large-scale hydropower production in Québec, Canada. To predict reservoir inflows, Hydro-Québec uses a lumped hydrological model named HSAMI (Bisson and Roberge, 1983, Fortin, 2000, St-Hilaire et al., 2003, Minville et al., 2008; 2009). The latter also uses an empirical temperature-based formulation to compute ET_p, hereby designed as Hydro-Québec model:

$$ET_{p,HQ} = \left[0.029718DTR\exp\left(0.0342DTR + 1.216\right)\right] \quad (5)$$

where DTR [°C] is the daily temperature range equal to the difference between the maximum and minimum air temperatures of the day; and $ET_{p,HQ}$ [mm] is the daily cumulative ET_p. To adjust the daily $ET_{p,HQ}$ to an hourly rate, a conversion factor is applied for each hour of the day. This conversion procedure is identical to that used for hourly computations with HSAMI (Fortin, 2000). While daily $ET_{p,HQ}$ has been shown to reproduce observations obtained with energy budget methods fairly well (Dionne et al., 2008; Isabelle, 2014), the conversion procedure to hourly scale adds uncertainty to the already empirical Hydro-Québec equation. Note that this temperature-based ET_p formulation has been shown to seriously overestimate ET_a in future climate predictions (Ludwig et al., 2009).

Conversion to modeled ET_a

For our study, each model described in Equations 2, 4 and 5 is multiplied by a scale factor denoted α. With the three models, α is taken as the ratio ET_a / ET_p to obtain $ET_{a,PM}$, $ET_{a,PT}$ and $ET_{a,HQ}$. In several studies, it is common practice to use such a coefficient for the Priestley-Taylor model, using a value of 1.26 for well-watered surfaces (Priestley and Taylor, 1972; Eichinger et al., 1996). Here, we used α as a calibration parameter to adjust modeled ET_p to observed ET_a values.

In this study, to compare modeled and observed ET_a, we used a fixed value of α for the whole study period. This is a simplification as α is known to vary over time. Over the course of three months, we feel that such variation should be negligible. We tested two of these values for each model: (i) an optimized value (α_{opt}) obtained as the value that minimize the root mean square error between observed ($ET_{a,EC}$) and modeled ET_a values (done for both daily and hourly values); and (ii) a value taken as the average of several α-coefficients obtained in a number of studies on peatland ET_a (α_{lit}) (see the literature review in Table 2). α_{opt} is considered to be the real value of α, while α_{lit} reproduces what a modeler without any direct ET_a observations would probably use. Table 3 presents the α used for each model. Note that as there are not many references on the Hydro-Québec model, we selected an α_{lit} of 0.75, a mean value commonly used in some unpublished HYDROTEL applications.

Performance metrics

To quantify the performance of each modeled ET_a when compared with $ET_{a,EC}$, we used the coefficient of determination R^2, the root mean squared error (RMSE), the mean bias (MB) and the Nash-Sutcliffe efficiency (NSE) (Nash and Sutcliffe, 1970). R^2 expresses the correlation between modeled and observed ET_a by describing the proportion of the variance in the observations that can be explained by the model. RMSE is an always positive expression of the error between observations and the model that is given in the units of ET_a, mm. MB differs from RMSE by taking positive or negative values. A perfect model would get both RMSE and MB equal to zero, with an R^2 of 1. RMSE and MB are particularly useful as they can be used to fraction the error between its systematic component (MB^2) and a random component (variance of the error, i. e. $RMSE^2 - MB^2$).

Impacts of ET_a precision on hydrological modeling

Hydrological model: HYDROTEL

To model the Necopastic peatland streamflow, we used the hydrological model HYDROTEL (Fortin et al., 2001a; Turcotte et al., 2003; Turcotte et al., 2007). It is a physically-based semi-distributed model simulating water flows in subsections of the watershed called relatively homogeneous hydrological units (RHHUs). These units are usually delineated using PHYSITEL (Turcotte et al., 2001; Rousseau et al., 2011; Noël et al., 2014), a specialized geographic information system used for watershed and stream network delineation as well as to determine other attributes needed to support distributed hydrological models. To create the RHHUs, PHYSITEL uses a digital elevation model, along with land cover and soil type maps. HYDROTEL has been successfully applied on many midlatitude watersheds (Fortin et al., 2001b; Lavigne et al., 2004; Boucher et al., 2011; Bouda et al., 2012; Ricard et al., 2012; Abaza et al., 2013, 2014; Bouda et al., 2014; Abaza et al., 2015), including the present field site (Clerc, 2009; Jutras et al., 2009). Note that the small Necopastic peatland is modeled with a single RHHU (see Figure 1b).

Once the digital renderings of the watershed landscapes and hydrological routes are made, HYDROTEL simulates six different components of the water cycle: (i) precipitation, by weather data interpolation; (ii) snowpack evolution; (iii) potential evapotranspiration; (iv) soil moisture balance; (v) surface runoff; and (vi) river routing. Each of these components can be simulated with different functions. In our case, we respectively used the following: (i) Thiessen polygons; (ii) no snowpack module necessary (snow-free period); (iii) measured ET_a and the three ET_p models described in the ET_p *models* section; (iv) three-layer vertical budget; (v) kinematic wave and (vi) kinematic wave. HYDROTEL runs each of these modules sequentially for each RHHU.

HYDROTEL can only be given ET_p inputs, from which it will determine ET_a based on soil and vegetation properties. The top soil layer is subject to bare-soil evaporation, computed as a function of ET_p, soil water content and vegetation leaf area index. Soil layers occupied by plant root systems lose water through transpiration, which is calculated as a function of soil moisture and the difference between ET_p and bare-soil evaporation. More details are available in Fortin et al. (2001a).

As part of the calibration procedure, HYDROTEL has a built-in set of 26 RHHU-independent parameters. One of them is a coefficient to modulate ET_p. Given that this study focuses on the sensitivity of the model to ET_p inputs, the calibration parameter for ET_p *within* HYDROTEL was set to 1. In our case, the precipitation module used for weather data interpolation is not activated since we have only one weather station (the flux tower, Figure 1c). The snowpack evolution module is also irrelevant given that our study focuses on the snow-free period. Therefore, the number of calibration parameters reduces to 13.

Due to the short study period, calibration was performed on the whole dataset (24 June to 27 September 2012), implying that no validation was performed. Taking the values of calibration parameters found manually by Jutras et al. (2009) for the same watershed as a starting point, we were able to obtain an improved manual calibration for our specific dataset. We obtained this parameter set by a trial-and-error parameter-by-parameter method focused on reducing the NSE between observed and modeled discharges. From this improved calibration parameter set, we used an automatic calibration algorithm to perform the multiple optimization described in the *Sensitivity analysis* section: the dynamically dimensioned search (DDS) algorithm (Tolson and Shoemaker, 2007). In brief, DDS searches for an optimized solution by randomly varying a selection of parameters and keeping only the variations that improve the NSE. The varied parameters are selected randomly, and the size of that varied parameter subset decreases as the algorithm approaches the user-set maximum number of iterations. The simplicity, low computational cost and high performance of DDS makes it ideal for use with HYDROTEL (Huot, 2014).

Given the limited duration of our study period, special care has to be given to the treatment of initial conditions, so that their impact on modeling results are minimized. Here, for each model run, a 1-month spin-up period was used with fixed hydrometeorological inputs. Moreover, the initial conditions of the model are included in the set of calibration parameters, and as such they are optimized. This particular procedure ensures that any modeling artifact related to the initial conditions are minimized. We are aware that the rather short duration of the modeling period is a limitation of the study, and only additional runs spanning over longer time periods will allow confirmation of our conclusions.

Sensitivity analysis

As described in Andréassian et al. (2004), two categories of sensitivity analyses can be used to quantify the impact of the precision of ET_p values on the hydrological modeling: static and dynamic.

With the static analysis, a benchmark set of calibration parameter values is obtained with the most precise ET available, in our case $ET_{a,EC}$. The simulated flows obtained with the benchmark calibration can be compared with the observed flows to assess the performance of the simulation. This sets the benchmark performance of the model and is usually done with objective functions (in our case, NSE, see the next section). Once the benchmark calibration was completed, the values of calibration parameters remained constant independently of the ET_p (either one of $ET_{p,PM}$, $ET_{p,PT}$ or $ET_{p,HQ}$) model used in subsequent simulations. The performance values of these other simulations were compared with the benchmark performance to assess the sensitivity of the hydrological model to ET_p inputs.

The dynamic analysis uses the same benchmark set of calibration parameter values obtained with $ET_{a,EC}$, with associated benchmark performance obtained by comparison of simulated with observed flows. In this instance however, recalibration is permitted, that is the values of the calibration parameters were optimized each time a different ET_p model was used.

As Andréassian et al. (2004) mentioned, the two types of sensitivity analysis stem from different modeling philosophies: the static approach assumes the existence of a "true" set of parameter values for a specific watershed, independently of climatic input data, whereas with the dynamic version, the values of the calibration parameters are allowed to "adapt" to varying climate inputs.

For this study, we performed both the static and dynamic input-related sensitivity analyses. The static analysis was performed with the benchmark calibration taken as that obtained by DDS using $ET_{a,EC}$ as the input. Since HYDROTEL can only be fed with ET_p values, we generated a synthetic time series, hereby labeled $ET_{p,EC}$. This synthetic ET_p was obtained as the input that ultimately led HYDROTEL to compute a modeled ET_a identical to the observations, $ET_{a,EC}$. Changing only ET_p inputs for subsequent simulations provided information on how sensitive HYDROTEL was with respect to simulated streamflow on small spatiotemporal scales.

The dynamic analysis was then performed using DDS to recalibrate the hydrological model each time ET_p inputs were changed. The recalibration allowed us to quantify how HYDROTEL could adapt to these changes in ET_p in terms of calibration parameter values. Both static and dynamic analyses were accomplished at the daily and hourly timescale.

Performance metrics and comparison criterion

To compare modeled and observed streamflow at the watershed outlet, we used RMSE to assess precision and accuracy of the model and NSE as a skill score. As previously mentioned, the objective function used in both manual and automatic calibration of HYDROTEL is the NSE.

To compare performance values of HYDROTEL using $ET_{p,EC}$ with those of HYDROTEL using ET_p models, we need to determine if the differences in performance metrics are significant. This is done with a comparison criteria. For comparisons of NSE, Nash and Sutcliffe (1970) already provided such a criterion named r^2:

$$r^2[\%] = \frac{\mathrm{NSE_{mod}} - \mathrm{NSE_{obs}}}{1 - \mathrm{NSE_{obs}}} \times 100 \quad (6)$$

where NSE_{mod} is the NSE obtained with the hydrological model when using modeled ET_p inputs; and NSE_{obs}, the NSE obtained when using $ET_{p,EC}$ inputs. If r^2 is negative, performance of the hydrological model is decreasing with modeled ET_p inputs, and inversely. Senbeta et al. (1999) suggest that values of $|\ r^2\ | > 10\%$ indicate a significant difference in performance. Note however that this threshold does not imply a formal statistically significant difference.

To compare RMSE values, we simply use the relative difference between the metrics:

$$\mathrm{RMSERD}[\%] = \frac{\mathrm{RMSE_{obs}} - \mathrm{RMSE_{mod}}}{\mathrm{RMSE_{obs}}} \times 100 \quad (7)$$

where $RMSE_{obs}$ is the RMSE obtained with the hydrological model when using $ET_{p,EC}$ inputs; and $RMSE_{mod}$, the RMSE obtained when using modeled ET_p inputs. Again, negative values indicate a decrease in performance with the use of modeled ET_p as inputs, and inversely.

Results

Measured water budget

Figure 2 presents the components of the water budget (Equation 1) measured at the Necopastic peatland field site. As expected, it highlights the annual cycle of ET_a, peaking at the summer solstice and slowly decreasing towards fall. On 9 September, our instruments measured very low ET_a; this day was characterized by a constant (but weak) rain all day long, with quite low solar radiation. Such conditions are known to stifle evaporation, and this phenomenon is amplified by shorter days and lower air temperatures. In general, ET_a rates (between 0.5 and 4.3 mm d^{-1}) are in line with those reported for summer at other boreal peatlands (Kellner, 2001; Humphreys et al., 2006; Wu et al., 2010; Brümmer et al., 2012; Runkle et al., 2014).

Figure 2 also illustrates how every term of the water budget reacts to precipitation. ET_a decreases during precipitation, but increases shortly after. S and Q are very sensitive to precipitation inputs, with a reaction time within a 30-min period. This reaction time is consistent with the watershed 10 to 20-min concentration time calculated using classical empirical formulations (Kirpich, 1940; Chow, 1962; Watt and Chow, 1985).

Streamflows exiting the watershed, Q, range between 0.3 and 6.7 mm d^{-1}, while ET_a rates are between 0.5 and 4.3 mm d^{-1}. In the absence of precipitation, these water outflows are in general very well balanced by a consequent decrease in groundwater storage, leading to almost no residual (i.e. with the average of daily values when $P = 0$: $ET_a = 2.75$ mm; $Q = 0.62$ mm; $S = -3.31$ mm; Residual = 0.06 mm). However, during rainfall, the groundwater storage increase exceeds $P - ET_a - Q$, leading to a negative residual (i.e. with the average of daily values when $P \neq 0$: $P = 3.36$ mm; $ET = 2.16$ mm; $Q = 0.99$ mm; $S = 1.89$ mm; Residual = −1.68 mm). This lack of equilibrium may be caused by the non-measured presence of groundwater inflows to the peatland; although measurement uncertainties to every water budget term may also be tied to such behavior.

To ascertain the influence of groundwater flow to Q, we have analyzed five rainfall events (3, 11, 14 , 30 July and 5 August) and performed a hydrograph separation into baseflow and quickflow. We used the standard graphical method outlined by Linsley et al. (1975), where baseflow during the hydrograph rise and fall following a precipitation event is assumed to vary exponentially. Quickflow is presumed to happen between the start of the rainfall event and the inflection point of the recession limb. For these events, the proportion of Q attributable to baseflow varied between 60% and 88%. Also, in the presence of quickflow (between 10 h and 32 h after the start of the rainfall events), the cumulated discharge amounted for 10% to 25% of the total precipitation, meaning that the latter mostly infiltrates the peatland and is not directly discharged.

The few instances where the residual takes high negative values (e.g. 3 July, 17 August, and 7 September) are caused by an important increase in groundwater storage that exceeds the incoming precipitation. Underestimation of incoming precipitation under windy conditions is a well-documented problem (e.g. Rodda and Dixon, 2012) that can be causing this feature. A positive peak of the residual is also noticeable at the end of the season (23 September). On this day, a 20-mm rainfall occurred while the water table was at its highest point of the season (~30 mm below the surface), implying that there may have been runoff not measured by the trapezoidal flume.

Figure 3 presents each term of the water budget on a cumulative basis, thus expressing the total seasonal volumes of water carried by each of these processes. The most noticeable feature is that ET_a is the largest term of the water budget with a cumulative value of 224 mm. P follows with 203 mm, and the other terms are much lower (Q, 78 mm; and S, 4 mm). The total seasonal residual is of −106 mm, meaning that measured water fluxes exiting the watershed during the summer also exceed those coming in. Again, a physically-reasonable hypothesis for this phenomenon can be the presence of groundwater flow coming into the peatland from areas where volumes of stored water from earlier snowmelt or rain are larger.

Comparison of modeled ET_a with observations

This part of our analysis describes the performance of each modeled ET_a with respect to the observations from the eddy flux tower. Figure 4 presents side-by-side comparisons of modeled (y-axis) and observed (x-axis) ET_a for the three models (Penman, Priestley-Taylor, Hydro-Québec), two α-coefficients (α_{opt} and α_{lit}), and two time steps (hourly and daily). Evidently, R^2 does not change with the different α-coefficients as it is invariant to a multiplication by a constant. Potential outliers calculated with the Cook's distance method (Cook, 1977; 1979; Montgomery et al., 2001) are identified as "X". Note that these outliers are not removed to calculate performance metrics and linear regressions. Table 4 presents the related performance metrics. For most modeled ET_a and α-coefficients, most of the error is random (i.e., $MB^2 \sim 0$, $RMSE^2 \sim$ variance of the error), meaning that the different versions of modeled ET_a express a variation in precision while accuracy is almost optimal. Finally, Figure 5 shows the time series of cumulative observed and modeled ET_a for both α-coefficients.

The Priestley-Taylor model seems to best represent observed ET_a both at the daily and hourly time scales, closely followed by the Penman model, whereas the Hydro-Québec is markedly behind, as shown by the R^2, RMSE and NSE values. Indeed, at the daily scale, with α_{opt}, R^2 varies between 0.90, 0.76 and 0.62, RMSE, between 0.50, 0.54 and 0.82, while NSE varies between 0.74, 0.70 and 0.32, for Priestley-Taylor, Penman and Hydro-Québec, respectively (Table 4). The hourly scale yields similar results. However, the Penman model is the least biased (e. g. on a daily scale, MB: −0.10 vs. −0.20 and −0.28 for Priestley-Taylor and Hydro-Québec, respectively). On a daily basis, the Penman model performance are fairly sensitive to outliers. Indeed, if the latter are excluded, some performance metrics increase above those of the Priestley-Taylor model without its own outliers (e. g. R^2: 0.83 vs. 0.89; RMSE: 0.47 vs. 0.51 mm; NSE: 0.78 vs. 0.74 for Penman without outliers and Priestley-Taylor without outliers, respectively).

Figure 4 clearly shows that the Hydro-Québec model obtains the poorest agreement with observations, as shown by the lower R^2 values (i.e. daily scale: 0.62; hourly scale: 0.69) and the other performance metrics (Table 4), especially on a daily scale. These results are expected from a temperature-based modeled ET_a. The model however obtains the best linear regression slope on a daily basis (0.99), but the large negative y-intercept reflects the important bias of the model.

Our results demonstrate that the α_{lit} scale factors are marginally decreasing the quality of estimation of the Penman and Priestley-Taylor models when compared to α_{opt}. This can be seen in the values of every performance metrics (see Table 4), where daily values decrease marginally while hourly values are still reasonably affected.

Figure 5 displays the differences in seasonal evaporated water at the watershed scale between modeled ET_a and observations. On a daily basis, total evaporated water of modeled ET_a are much closer to the 224 mm (see dashed horizontal line in Figure 5) of observed $ET_{a,EC}$ when α_{opt} is used, especially for the Penman and Priestley-Taylor models. The Hydro-Québec model is unaffected by the change in α-coefficient since values are almost identical (see Table 3). The same can be said for the Priestley-Taylor model on a daily basis. An opposite behavior can be seen on an hourly basis, where Penman and Priestley-Taylor depths of water are more realistic with α_{lit}. With α_{opt}, the worst model is the Priestley-Taylor model, underestimating the total evaporated height of water by about 50 mm. It appears to diverge from the Penman model around the middle of August (Figure 5c). This behavior is visible with α_{lit}, and on a daily basis, where it diverges from observations around the same time.

Impacts of ET_a precision on hydrological modeling

Figure 6 shows the hydrographs of observed and modeled streamflow when $ET_{p,EC}$ and each version of modeled ET_p are used as input. Table 5 presents the values of performance metrics for each combination of timescale and ET_p inputs, and for both static and dynamic sensitivity analyses.

HYDROTEL reproduces observed discharges fairly well when fed the best representation of ET_p possible (e.g. at the daily scale, with $ET_{p,EC}$, RMSE: 0.32 mm; NSE: 0.89). Figure 6 shows this as well, although the model seems slightly overreactive to precipitation and dry periods. Visual inspection of the hydrographs shows that the curves obtained with modeled ET_p follow the same behavior, showing that the model dynamic remains the same with different ET_p inputs.

Table 6 presents a detailed summary of the differences in watershed model efficiency (via the comparison criteria RMSERD and r^2), when varying the ET_p inputs with the Penman, Priestley-Taylor and Hydro-Québec models. Bolded values of r^2 imply a significant difference according to Senbeta et al. (1999) criteria (>|10%|). The table shows results for both static and dynamic sensitivity analyses.

The static sensitivity analysis (Table 6, left side) shows that HYDROTEL performance significantly decreases when ET_p inputs are changed, especially with the Priestley-Taylor and Hydro-Québec models. When the Penman model is used, streamflow simulated with HYDROTEL are in closer agreement with observed flows, but still significantly off. With the modeled ET_p and without recalibration (see dashed colored lines in Figure 6), the hydrographs simulated by HYDROTEL start to diverge from the curve generated with $ET_{p,EC}$ (see dashed black line in Figure 6) around 5 July, with a positive shift of around 0.2-0.5 mm d^{-1}, depending on the ET_p model. These results provide information on the internal sensitivity of HYDROTEL to ET_p inputs, which is high without recalibration.

This last conclusion does not systematically emerge from the dynamic sensitivity analysis (Table 6, right side). When recalibration is allowed with each ET_p input, it compensates accordingly and bring performance values closer to, or even over those obtained with $ET_{p,EC}$. Indeed, the hydrographs obtained by HYDROTEL with modeled ET_p during the dynamic sensitivity analysis (see solid colored lines in Figure 6) are virtually superimposed over the curve simulated with $ET_{p,EC}$ (black dashed line in Figure 6). Results show that HYDROTEL has an efficiency more comparable to the Priestley-Taylor model than with $ET_{p,EC}$ (e.g., at the hourly scale, RMSE: 0.015 vs 0.015 mm; NSE: 0.88 vs 0.87). Meanwhile, the use of the Penman model creates a very slight drop in HYDROTEL performances. Surprisingly, with the temperature-based Hydro-Québec model, simulated flows have the same agreement with observed flows than with $ET_{p,EC}$ at both daily scale and hourly scale (e.g., at the hourly scale, RMSE: 0.015 mm; NSE: 0.87).

Discussion

Comparison of modeled ET_a with observations

The fact that the Priestley-Taylor model performs similarly to the Penman model on a side-by-side comparison with observations seems to contradict the general idea that the efficiency of a model is proportional to the number of key physical processes considered. Indeed, the Penman model is expected to be more accurate than the Priestley-Taylor model by taking into account the effects of vapor pressure deficit and, hence, air advection: a crucial component of the ET_a process (e.g. Donohue et al., 2010). However, Drexler et al. (2004) mention that the Penman model can be questionable when applied to peatlands because of a high surface vegetation variability.

On a Swedish peatland, Kellner et al. (2001) reported that a low coupling between ET_a and ambient vapor pressure deficit is the reason behind the efficiency of the Priestley-Taylor model with a fixed α-coefficient. A similar phenomenon happens at our field site: ET_a and ambient vapor pressure deficit are poorly correlated (R^2 = 0.43). However, a previous study at this particular field site determined that ET_a has a good correlation (R^2 = 0.70) with the difference in humidity between the soil surface and the air aloft (Isabelle et al., 2015). Thus, the surface humidity appears to have a much more important control on ET_a than the humidity of the ambient air. However, the fact that the Priestley-Taylor model neglects air advection is a possible explanation for the visible differences in ET_a after mid-August, when net radiation starts to decrease substantially at these latitudes.

According to our results, the Hydro-Québec model is the least precise of our modeled ET_a when compared to observations. However, it seems that the empirical constants of the Hydro-Québec model and its functional form are well-suited for the subarctic regions east of the James Bay, since R^2, RMSE and NSE values are still reasonable. Isabelle (2014) shows that this model does not work as well on other peatlands in the St. Lawrence River lowlands or Western Great Plains of Canada, characterized by much different climates.

The good performance of Penman and Priestley-Taylor models with α_{lit} are not surprising since the respective values of α_{opt} and α_{lit} are relatively close, especially on a daily basis (Table 3). Plus, it appears that our method to obtain α_{opt} on an hourly basis produces values that underestimates total seasonal volumes. If we instead compute α as the ratio between observed and modeled total seasonal volume, we obtain values of 0.59, 0.92 and 0.87 for the Penman, Priestley-Taylor and Hydro-Québec models, respectively. However, these values yield much lower side-by-side performance (results not shown).

Nevertheless, this is excellent news to modelers that rarely have access to detailed ET_a measurements for a given boreal peatland site. For them, the use of a fixed α scale factor to convert ET_p to ET_a with values of the order of 0.63 for Penman and 0.84 for Priestley-Taylor seems indicated in boreal peatlands, especially to reproduce seasonal volumes. The same cannot be said for the Hydro-Québec model. Caution needs to be exercised if the temperature-based model is to be used to model ET_a, as a coarse adjustment can lead to serious seasonal volume offset.

Impacts of ET_a precision on hydrological modeling

In some cases, our results show that HYDROTEL can generate slightly more representative streamflows with ET_p models than with observations. The ensuing HYDROTEL efficiency highlights the capacity of the calibration parameter values to adapt to different hydrometeorological inputs. For example, despite some important differences in precision between $ET_{a,EC}$ and $ET_{a,HQ}$ (e.g., at the hourly scale and with α_{opt}, RMSE: 0.063 mm; NSE: 0.63), recalibration of HYDROTEL provides a way to find a set of parameter values capable of compensating for those differences, providing satisfying streamflows. This adaptive behavior can be generalized to all studied ET_p models. This feature is especially highlighted in Figure 6, where flows generated during the dynamic analysis with every ET_p models are virtually identical to those obtained with $ET_{p,EC}$. Of course, the calibration procedure becomes very efficient considering that it is performed using the whole sampling period. Our observations may not hold at larger time scales. However, the results follow a similar trend at the hourly scale, where a much larger data sample is used.

It is also important to remember that $ET_{a,EC}$ observations are not a perfect representation of ET_a. The method of Finkelstein and Sims (2001) estimates that eddy covariance uncertainties related to random sampling errors amount to about 12% of the season total evaporated water. Furthermore, some uncertainties also lie in the assumption that $ET_{a,EC}$ is representative of the whole watershed ET_a. Using the Kljun et al. (2004) model, the flux tower mean footprint for the whole season is of the order of 1 ha while the watershed area is 97 ha. Our assumption stems from the fact that most of the Necopastic peatland watershed is covered with the same type of surface as that found within the footprint of the flux tower (peatlands covering 63% of the watershed area). The other land covers of the watershed area, mostly boreal forest, probably have different ET_a rates. Another possible source of uncertainties for eddy covariance measurements lies in a well-documented problem: the failure to close the energy balance (Foken, 2008). Our observations show that turbulent fluxes ($H + LE$) account for only 70% of the total available energy ($R_n - G$) for our whole study period, a value within the range of turbulent fluxes observed at other sites (Wang and Dickinson, 2012). This means that $ET_{a,EC}$ may underestimate actual rates. These uncertainties on observed ET_a may play a role in the improvements of HYDROTEL efficiency using ET_p models.

Several other studies have reported that the precision of ET_p values does not excessively affect the efficiency of a given hydrological model (see Table 1). However, none of them have used ET_a observations as the best estimates to model streamflow. According to our results, the modeled ET_a are reasonably close to the observed rates. These estimations are good enough for short-term streamflow simulations, especially considering that the calibration of the hydrological model is able to adapt to different ET_p inputs. Discrepancies in observed and modeled ET_a rates are also uninfluential compared to precipitations driving the hydrological model.

This study focused on much smaller spatiotemporal scales than what was previously reported. The fact that the time of concentration of the watershed is relatively short required an hourly computational time step. ET_a rates vary greatly during the day, meaning that hourly estimates could be relevant for streamflow modeling. This is especially true for peatlands, known to lose a lot of water through ET_a. At the hourly timescale, the modeled ET_a reproduced observations with good precision, albeit not as good as at the daily timescale. This good performance is seen even for the empirical Hydro-Québec model, which was originally designed for a daily timescale. Meanwhile, HYDROTEL has no difficulty to cope with different hourly ET_p inputs for modeling hourly streamflow during a single summer.

These results appear to confirm those of previous studies summarized in Table 1. The precision of ET_p does not seem to have an impact on the efficiency of streamflow modeling, even at smaller spatial and temporal scales, and even if precise ET_a observations are used as benchmark. These results are more indicative than conclusive, given that they were obtained at a single field site over a relatively short study period.

On the surface, this seems to point to the use of more simple temperature-based ET_p models for hydrological modeling or forecasting. However, these models need to be used cautiously as their calibration (i.e., empirical constants and functional forms) still needs to be optimal. Spatiotemporal transferability of the calibration of these temperature-based ET_a formulations are also questionable (Mauser and Bach, 2009; Lofgren et al., 2011; Hoerling et al., 2012), including for the Hydro-Québec model (Ludwig et al., 2009).

Conclusion

The goal of this study was to compare three ET_p models of contrasting complexities with precise field observations, and to assess the impacts of using these models on the efficiency of a physically-based hydrological model. The study focused on a small watershed (0.97 km^2) dominated by a boreal peatland, a type of environment prone to substantial evapotranspiration. Our analysis relied on an original dataset of eddy covariance fluxes and other meteorological and hydrological variables measured during summer 2012.

As expected, in terms of side-by-side comparisons between observed and modeled ET_a, the combinational and radiation-based models (Penman and Priestley-Taylor) had better performance than the temperature-based Hydro-Québec model. However, a previously reported low coupling between ET_a and ambient vapor pressure deficit benefited the Priestley-Taylor model when compared to the more comprehensive Penman model. Nevertheless, the Priestley-Taylor model seemed to diverge from observed data by the end of the summer, seriously underestimating ET_a. Results of the Penman and Priestley-Taylor models were adjusted from ET_p to ET_a according to an α-coefficient coming from a literature review on boreal peatlands (Penman: 0.63; Priestley-Taylor: 0.84), but it did not affect the models respective efficiencies, compared to an optimized α-coefficient. On an hourly basis, it was even a better value to compute seasonal evaporated volumes.

While each ET_p model reproduced observed values with different precisions, they did not have an important impact on the hydrological modeling of streamflows at the watershed outlet when compared to those simulated using ET_a observations. A static sensitivity analysis established that HYDROTEL can be very sensitive to ET_p. This sensitivity was greatly diminished in the dynamic sensitivity analysis, when recalibration was performed with each ET_p inputs. In other words, the sensitivity was almost nullified by adjusting the values of the calibration parameters, at least on a very short hydrological modeling period. Altogether, the results of this study illustrated that the set of calibration parameters has a substantial short-term capacity to offset the precision of ET_p inputs.

This study illustrates that, for a small peatland-dominated watershed and a short modeling period, the precision of ET_p inputs does not seem to affect the modeling of streamflows at the outlet with HYDROTEL. This conclusion still needs to be confirmed with a longer modeling period to affect operational modeling strategies. The simplicity of a temperature-based ET_p model appears enticing, provided that it is properly calibrated. However, the transposability of the above results to larger spatiotemporal scales still needs to be confirmed.

Acknowledgements

The authors would like to acknowledge the Cree Nation of Chisasibi along with Hank A. Margolis, Carole Coursolle, Simone Grindat, Sébastien Lambert-Girard, Gabriel Hould-Gosselin, Mathieu Oreiller, Maxime Fossey, Claudine Fortier and Catherine Guay for their collaboration with the field campaign. We thank Gwenael Carrer and Clément Clerc for their previous work and their data on this field site. We would also like to thank Annie Poulin, Pierre-Luc Huot, Stéphane Savary, Sébastien Tremblay and Sylvain Jutras for their assistance with DDS and HYDROTEL, and Annie-Claude Parent for the preparation of the site map. This work was supported by Ouranos (consortium on regional climatology and adaptation to climate change), the Natural Sciences and Engineering Research Council of Canada and the Canadian Foundation for Climate and Atmospheric Sciences.

References

Abaza, M., Anctil, F., Fortin, V., and Turcotte, R. 2013. A comparison of the Canadian global and regional meteorological ensemble systems for short-term hydrological forecasting. Monthly Weather Reviews, **141**: 3462-3476. doi:10.1175/MWR-D-12-00206.1.

Abaza, M., Anctil, F., Fortin, V., and Turcotte, R. 2014. Sequential streamflow assimilation for short-term hydrological ensemble forecasting. Journal of Hydrology, **519**: 2692-2706. doi:10.1016/j.jhydrol.2014.08.038.

Abaza, M., Anctil, F., Fortin, V., and Turcotte, R. 2015. Exploration of sequential streamflow assimilation in snow dominated watersheds. Advances in Water Resources, **80**: 79-89. doi:10.1016/j.advwatres.2015.03.011.

Admiral, S. W., Lafleur, P. M., and Roulet, N. T. 2006. Controls on latent heat flux and energy partitioning at a peat bog in eastern Canada. Agricultural and Forest Meteorology, **140**: 308-321. doi:10.1016/j.agrformet.2006.03.017.

Andersson, L. 1992. Improvements of runoff models: what way to go? Nordic Hydrology, **23**: 315-332.

Andréassian, V., Perrin, C., and Michel, C. 2004. Impact of imperfect potential evapotranspiration knowledge on the efficiency and parameters of watershed models. Journal of Hydrology, **286**: 19-35. doi:10.1016/j.jhydrol.2003.09.030.

Aselmann, I., and Crutzen, P. J. 1989. Global distribution of natural freshwater wetlands and rice paddies, their net primary productivity, seasonality and possible methane emissions. Journal of Atmospheric Chemistry, **8**: 307-358. doi:10.1007/BF00052709.

Bisson, J., and Roberge, F. 1983. Prévisions des apports naturels: Expérience d'Hydro-Québec. *In* Workshop on flow predictions. Toronto, Canada: Institute of Electrical and Electronics Engineers (IEEE).

Boucher, M.-A., Anctil, F., Perreault, L., and Tremblay, D. 2011. A comparison between ensemble and deterministic hydrological forecasts in an operational context. Advances in Geosciences, **29**: 85-94. doi:10.5194/adgeo-29-85-2011.

Bouda, M., Rousseau, A. N., Gumiere, S. J., Gagnon, P., Konan, B., and Moussa, R. 2014. Implementation of an automatic calibration procedure for HYDROTEL based on prior OAT sensitivity and complementary identifiability analysis. Hydrological Processes, **28**: 3947-3961. doi:10.1002/hyp.9882.

Bouda, M., Rousseau, A. N., Konan, B., Gagnon, P., and Gumiere, S. J. 2012. Bayesian uncertainty analysis of the distributed hydrological model HYDROTEL. Journal of Hydrologic Engineering, **17**: 1021-1032. doi:10.1061/(ASCE)HE.1943-5584.0000550.

Bridgham, S. D., Pastor, J., Dewey, B., Weltzin, J. F., and Updegraff, K. 2008. Rapid carbon response of peatlands to climate change. Ecology, **89**: 3041-3048. doi:10.1890/08-0279.1.

Brümmer, C., Black, T. A., Jassal, R. S., Grant, N. J., Spittlehouse, D. L., Chen, B., Nesic, Z., Amiro, B. D., Arain, M. A., and Barr, A. G. 2012. How climate and vegetation type influence evapotranspiration and water use efficiency in Canadian forest, peatland and grassland ecosystems. Agricultural and Forest Meteorology, **153**: 14-30. doi:10.1016/j.agrformet.2011.04.008.

Brutsaert, W. 1982. Evaporation into the Atmosphere: Theory, History, and Applications. Reidel, Dordrecht, Netherlands.

Brutsaert, W. 2005. Hydrology: an Introduction. Cambridge University Press, Cambridge, MA.

Campbell, D. I., and Williamson, J. 1997. Evaporation from a raised peat bog. Journal of Hydrology, **193**: 142-160. doi:10.1016/S0022-1694(96)03149-6.

Chow, V. T. 1962. Hydrological Determination of Waterway Areas for the Design of Drainage Structures in Small Drainage Basins. Engineering Experiment Station Bulletin, 462, University of Illinois, Urbana, IL.

Clerc, C. 2009. Suivi de la nappe, de la recharge et de l'écoulement à l'aide de méthodes in situ afin de comprendre la dynamique des tourbières ombrotrophes de la région de la Baie James. M.Sc. thesis, Institut national de la recherche scientifique - Centre Eau Terre Environnement, Québec, QC.

Cook, R. D. 1977. Detection of influential observations in linear regression. Technometrics, **19**: 15-18. doi:10.2307/1268249.

Cook, R. D. 1979. Influential observations in linear regression. Journal of the American Statistical Association, **74**: 169-174. doi:10.2307/2286747.

Dionne, F.-L., Ciobanas, A. I., and Rousseau, A. N. 2008. Validation d'un modèle de rayonnement net et comparaison de l'équation d'Hydro-Québec avec le bilan d'énergie thermique de surface. Research report R-1036, Institut national de la recherche scientifique – Centre Eau Terre Environnement, Québec, QC.

Dise, N. B. 2009. Peatland response to global change. Science, **326**: 810-811. doi:10.1126/science.1174268.

Donohue, R. J., McVicar, T. R., and Roderick, M. L. 2010. Assessing the ability of potential evaporation formulations to capture the dynamics in evaporative demand within a changing climate. Journal of Hydrology, **386**: 186-197. doi:10.1016/j.jhydrol.2010.03.020.

Drexler, J. Z., Snyder, R. L., Spano, D., and Paw U, K. T. 2004. A review of models and micrometeorological methods used to estimate wetland evapotranspiration. Hydrological Processes, **18**: 2071-2101. doi:10.1002/hyp.1462.

Eichinger, W. E., Parlange, M. B., and Stricker, H. 1996. On the concept of equilibrium evaporation and the value of the Priestley-Taylor coefficient. Water Resources Research, **32**: 161-164.

Finkelstein, P. L., and Sims, P. F. 2001. Sampling error in eddy correlation flux measurements. Journal of Geophysical Research, **106**: 3503-3509. doi:10.1029/2000JD900731.

Foken, T. 2008. The energy balance closure problem: An overview. Ecological Applications, **18**: 1351-1367. doi:10.1890/06-0922.1.

Fortin, J.-P., Turcotte, R., Massicotte, S., Moussa, R., Fitzback, J., and Villeneuve, J.-P. 2001a. Distributed watershed model compatible with remote sensing and GIS data. I: Description of model. Journal of Hydrologic Engineering, **6**: 91-99.

Fortin, J.-P., Turcotte, R., Massicotte, S., Moussa, R., Fitzback, J., and Villeneuve, J.-P. 2001b. Distributed watershed model compatible with remote sensing and GIS data. II: Application to Chaudière watershed. Journal of Hydrologic Engineering, **6**: 100-108.

Fortin, V. 2000. Le modèle météo-apport HSAMI: historique, théorie et application. Institut de recherche Hydro-Québec, Varennes, QC.

Fowler, A. 2002. Assessment of the validity of using mean potential evaporation in computations of the long-term soil water balance. Journal of Hydrology, **256**: 248-263. doi:10.1016/S0022-1694(01)00542-X.

Glaser, P. H., Hansen, B. C. S., Siegel, D. I., Reeve, A. S., and Morin, P. J. 2004. Rates, pathways and drivers for peatland development in the Hudson Bay Lowlands, northern Ontario, Canada. Journal of Ecology, **92**: 1036-1053. doi:10.1111/j.0022-0477.2004.00931.x.

Google Earth. 2017. Google Earth V 7.1.8.3036. Necopastic peatland watershed, Canada, 53°40'28"N, 78°10'14" W, eye altitude 2 km. Digital Globe 2017. Available from http://www.earth.google.com, (accessed 25 July 2017).

Gorham, E. 1991. Northern peatlands: role in the carbon cycle and probable responses to climatic warming. Ecological Applications, **1**(2): 182-195. doi:182.10.2307/1941811.

Halliwell, D. H., and Rouse, W. R. (1987). Soil heat flux in permafrost: characteristics and accuracy of measurement. Journal of Climatology, **7**: 571-584. doi:10.1002/joc.3370070605.

Hansson, K. and Lundin, L.C. 2006. Water content reflectometer application to construction materials and its relation to time domain reflectometry. Vadose Zone Journal, **5**(1): 459-468. doi:10.2136/vzj2005.0053.

Hoerling, M. P., Eischeid, J. K., Quan, X.-W., Diaz, H. F., Webb, R. S., Dole, R. M., and Easterling, D. R. 2012. Is a transition to semipermanent drought conditions imminent in the US Great Plains? Journal of Climate, **25**: 8380-8386. doi:10.1175/JCLI-D-12-00449.1.

Humphreys, E. R., Lafleur, P. M., Flanagan, L. B., Hedstrom, N., Syed, K. H., Glenn, A. J., and Granger, R. 2006. Summer carbon dioxide and water vapor fluxes across a range of northern peatlands. Journal of Geophysical Research, **111**(G04011). doi:10.1029/2005JG000111.

Huot, P.-L. 2014. Évaluation de méthodes d’optimisation pour le calage efficace de modèles hydrologiques coûteux en temps de calcul. M.Sc. thesis. École de technologie supérieure, Montréal, QC.

IPCC (Intergovernmental Panel on Climate Change). 2013. Climate Change 2013: The Scientific Basis Contribution of Working Group I to the Fifth Assessment Report of the Intergovernmental Panel on Climate Change. Cambridge University Press, Cambridge, MA.

Isabelle, P.-E. 2014. Simplification de l’estimation des taux d’évapotranspiration sur les tourbières boréales par la quasi-neutralité de l’atmosphère. M.Sc. thesis. Institut national de la recherche scientifique – Centre Eau Terre Environnement, Québec, QC.

Isabelle, P.-E., Nadeau, D. F., Rousseau, A. N., Coursolle, C., and Margolis, H. A. 2015. Applicability of the bulk-transfer approach to estimate evapotranspiration from boreal peatlands. Journal of Hydrometeorology, **16**: 1521-1539. doi:10.1175/JHM-D-14-0171.1.

Itier, B., and Brunet, Y. 1996. Recent developments and present trends in evaporation research: a partial survey. *In* Evapotanspiration and irrigation scheduling, Proceedings of the International Conference ASCE, San Antonio, TX, pp. 1-20.

Joukainen, S. 2000. Improving the calculation of potential evapotranspiration of the HBV model: application to the Ounasjoki watershed. In Nordic hydrological conference, Uppsala, Sweden, pp. 347-354.

Jutras, S., Rousseau, A. N., and Clerc, C. 2009. Implementation of a peatland specific water budget algorithm in HYDROTEL. Canadian Water Resources Journal, **34**: 349-364. doi:10.4296/cwrj3404349.

Katul, G. G., and Parlange, M. B. 1992. A Penman-Brutsaert model for wet surface evaporation. Water Resources Research, **28**: 121-126. doi:10.1029/91WR02324.

Kellner, E. 2001. Surface energy fluxes and control of evapotranspiration from a Swedish sphagnum mire. Agricultural and Forest Meteorology, **110**: 101-123. doi:10.1016/S0168-1923(01)00283-0.

Kellner, E., and Lundin, L. C. 2001. Calibration of time domain reflectometry for water content in peat soil. Nordic Hydrology, **32**(4-5), 315-332.

Kirpich, Z. P. 1940. Time of concentration of small agricultural watersheds. Civil Engineering, **10**: 362.

Kljun, N., Calanca, P., Rotach, M., and Schmid, H. 2004. A simple parameterisation for flux footprint predictions. Boundary-Layer Meteorology, **112**: 502-523. doi:10.1023/B:BOUN.0000030653.71031.96.

Koerselman, W., and Beltman, B. 1988. Evapotranspiration from fens in relation to Penman's potential free water evaporation (E_0) and pan evaporation. Aquatic Botany, **31**: 307-320. doi:10.1016/0304-3770(88)90019-8.

Kokkonen, T. S., and Jakeman, A. J. 2001. A comparison of metric and conceptual approaches in rainfall-runoff modeling and its implications. Water Resources Research, **37**: 2345-2352. doi:10.1029/2001WR000299.

Lafleur, P. M., Hember, R. A., Admiral, S. W., and Roulet, N. T. 2005. Annual and seasonal variability in evapotranspiration and water table at a shrub covered bog in southern Ontario, Canada. Hydrological Processes, **19**: 3533-3550. doi:10.1002/hyp.5842.

Lafleur, P. M., and Roulet, N. T. 1992. A comparison of evaporation rates from two fens of the Hudson Bay Lowland. Aquatic Botany, **44**: 59-69. doi:10.1016/0304-3770(92)90081-S.

Lavigne, M. P., Rousseau, A. N., Turcotte, R., Laroche, A. M., Fortin, J. P., and Villeneuve, J. P. 2004. Validation and use of a semi-distributed hydrological modeling system to predict short-term effects of clear-cutting on a watershed hydrological regime. Earth Interactions, **8**: 1-19. doi:10.1175/1087-3562(2004)008<0001:VAUOAS>2.0.CO;2.

Leclair, M., Whittington, P., and Price, J. S. 2015. Hydrological functions of a mine-impacted and natural peatland-dominated watershed, James Bay Lowland. Journal of Hydrology: Regional Studies, **4**: 732-747. doi:10.1016/j.ejrh.2015.10.006.

Linsley, R. K., Kohler, M. A., and Paulhus, J. L. H. 1975. Hydrology for engineers, McGraw-Hill, New York, NY.

Lofgren, B. M., Hunter, T. S., and Wilbarger, J. 2011. Effects of using air temperature as a proxy for potential evapotranspiration in climate change scenarios of Great Lakes basin hydrology. Journal of Great Lakes Research, **37**: 744-752. doi:10.1016/j.jglr.2011.09.006.

Ludwig, R., May, I., Turcotte, R., Vescovi, L., Braun, M., Cyr, J.F., Fortin, L.G., Chaumont, D., Biner, S., Chartier, I. and Caya, D. 2009. The role of hydrological model complexity and uncertainty in climate change impact assessment. Advances in Geosciences, **21**: 63-71. doi:10.5194/adgeo-21-63-2009.

Matthews, E., and Fung, I. 1987. Methane emission from natural wetlands: Global distribution, area, and environmental characteristics of sources. Global Biogeochemical Cycles, **1**: 61-86. doi:10.1029/GB001i001p00061.

Mauser, W. and Bach, H. 2009. PROMET–Large scale distributed hydrological modelling to study the impact of climate change on the water flows of mountain watersheds. Journal of Hydrology, **376**(3): 362-377. doi:10.1016/j.jhydrol.2009.07.046.

Minville, M., Brissette, F., and Leconte, R. 2008. Uncertainty of the impact of climate change on the hydrology of a nordic watershed. Journal of Hydrology, **358**: 70-83. doi:10.1016/j.jhydrol.2008.05.033.

Minville, M., Brissette, F., and Leconte, R. 2009. Impacts and uncertainty of climate change on water resource management of the Peribonka river system (Canada). Journal of Water Resources Planning and Management, **136**: 376-385. doi:10.1061/(ASCE)WR.1943-5452.0000041.

Montgomery, D. C., Peck, E. A., Vining, G. G. 2001. Introduction to Linear Regression Analysis, 3rd edition. John Wiley & Sons, New York, NY.

Nadeau, D. F., Rousseau, A. N., Coursolle, C., Margolis, H. A., and Parlange, M. B. 2013. Summer methane fluxes from a boreal bog in northern Quebec, Canada, using eddy covariance measurements. Atmospheric Environment, **81**: 464-474. doi:10.1016/j.atmosenv.2013.09.044.

Nandakumar, N., and Mein, R. G. 1997. Uncertainty in rainfall-runoff model simulations and the implications for predicting the hydrologic effects of land use change. Journal of Hydrology, **192**: 211-232. doi:10.1016/S0022-1694(96)03106-X.

Nash, J., and Sutcliffe, J. V. 1970. River flow forecasting through conceptual models 1: A discussion of principles. Journal of Hydrology, **10**: 282-290. doi:10.1016/0022-1694(70)90255-6.

Noël, P., Rousseau, A., Paniconi, C., and Nadeau, D. 2014. Algorithm for delineating and extracting hillslopes and hillslope width functions from gridded elevation data. Journal of Hydrologic Engineering, **19**: 366-374. doi:10.1061/(ASCE)HE.1943-5584.0000783.

NWGG (National Wetlands Working Group). 1997. The Canadian Wetland Classification System, 2nd Edition. Warner, B.G. and C.D.A. Rubec (eds.), Wetlands Research Centre, University of Waterloo, Waterloo, ON, Canada. 68 p.

Ochsner, T. E., Sauer, T. J., and Horton, R. 2007. Soil heat storage measurements in energy balance studies. Agronomy Journal, **99**: 311-319. doi:10.2134/agronj2005.0103S

Oudin, L., Hervieu, F., Michel, C., Perrin, C., Andréassian, V., Anctil, F., and Loumagne, C. 2005. Which potential evapotranspiration input for a lumped rainfall-runoff model? Journal of Hydrology, **303**: 290-306. doi:10.1016/j.jhydrol.2004.08.025.

Paavilainen, E., and Päivänen, J. 1995. Peatland forestry: Ecology and principles. Springer-Verlag, Berlin-Heideberg-New York.

Parmele, L. H. 1972. Errors in output of hydrologic models due to errors in input potential evapotranspiration. Water Resources Research, **8**: 348-359. doi:10.1029/WR008i002p00348.

Parmentier, F., Van der Molen, M., de Jeu, R., Hendriks, D., and Dolman, A. 2009. CO_2 fluxes and evaporation on a peatland in the Netherlands appear not affected by water table fluctuations. Agricultural and Forest Meteorology, **149**: 1201-1208. doi:10.1016/j.agrformet.2008.11.007.

Paturel, J., Servat, E., and Vassiliadis, A. 1995. Sensitivity of conceptual rainfall-runoff algorithms to errors in input data-case of the GR2M model. Journal of Hydrology, **168**: 111-125. doi:10.1016/0022-1694(94)02654-T.

Penman, H. L. 1948. Natural evaporation from open water, bare soil and grass. Proceedings of the Royal Society of London, **A193**: 120-145.

Petrone, R., Silins, U., and Devito, K. 2007. Dynamics of evapotranspiration from a riparian pond complex in the western boreal forest, Alberta, Canada. Hydrological Processes, **21**: 1391-1401. doi:10.1002/hyp.6298.

Petrone, R. M., Price, J. S., Waddington, J., and Von Waldow, H. 2004. Surface moisture and energy exchange from a restored peatland, Quebec, Canada. Journal of Hydrology, **295**: 198-210. doi:10.1016/j.jhydrol.2004.03.009.

Price, J.S., Branfireun, B.A., Michael Waddington, J. and Devito, K.J. 2005. Advances in Canadian wetland hydrology, 1999–2003. Hydrological Processes, **19**(1): 201-214. doi:10.1002/hyp.5774.

Priestley, C., and Taylor, R. 1972. On the assessment of surface heat flux and evaporation using large-scale parameters. Monthly Weather Reviews, **100**: 81-92.

Ricard, S., Bourdillon, R., Roussel, D., and Turcotte, R. 2012. Global calibration of distributed hydrological models for large-scale applications. Journal of Hydrologic Engineering, **18**: 719-721. doi:10.1061/(ASCE)HE.1943-5584.0000665.

Rodda, J.C. and Dixon, H. 2012. Rainfall measurement revisited. Weather, **67**(5): 131-136. doi:10.1002/wea.875.

Rouse, W. R. 1984. Microclimate at arctic tree line 3. The effects of regional advection on the surface energy balance of upland tundra. Water Resources Research, **20**: 74-78. doi:10.1029/WR020i001p00074.

Rouse, W. R., Hardill, S. G., and Lafleur, P. M. 1987. The energy balance in the coastal environment of James Bay and Hudson Bay during the growing season. Journal of Climatology, **7**: 165-179. doi:10.1002/joc.3370070207.

Rousseau, A., Fortin, J., Turcotte, R., Royer, A., Savary, S., Quévy, F., Noël, P., and Paniconi, C. 2011. PHYSITEL, a specialized GIS for supporting the implementation of distributed hydrological models. Water News – Official Magazine of the Canadian Water Resources Association, **31**: 18-20.

Runkle, B., Wille, C., Gažovič, M., Wilmking, M., and Kutzbach, L. (2014). The surface energy balance and its drivers in a boreal peatland fen of northwestern Russia. Journal of Hydrology, **511**: 359-373. doi:10.1016/j.jhydrol.2014.01.056.

Seiller, G., and Anctil, F. 2014. Climate change impacts on the hydrologic regime of a Canadian river: comparing uncertainties arising from climate natural variability and lumped hydrological model structures. Hydrology and Earth System Sciences, **18**: 2033-2047. doi:10.5194/hess-18-2033-2014.

Seiller, G., and Anctil, F. 2016. How do potential evapotranspiration formulas influence hydrological projections? Hydrological Sciences Journal, **61**: 2249-2266. doi:10.1080/02626667.2015.1100302.

Senbeta, D., Shamseldin, A., and O'Connor, K. 1999. Modification of the probability-distributed interacting storage capacity model. Journal of Hydrology, **224**: 149-168. doi:10.1016/S0022-1694(99)00127-4.

Sonnentag, O., Van der Kamp, G., Barr, A., and Chen, J. 2010. On the relationship between water table depth and water vapor and carbon dioxide fluxes in a minerotrophic fen. Global Change Biology, **16**: 1762-1776. doi:10.1111/j.1365-2486.2009.02032.x.

St-Hilaire, A., Ouarda, T. B., Lachance, M., Bobée, B., Gaudet, J., and Gignac, C. 2003. Assessment of the impact of meteorological network density on the estimation of basin precipitation and runoff: A case study. Hydrological Processes, **17**: 3561-3580. doi:10.1002/hyp.1350.

Tarnocai, C., Kettles, I.M., Lacelle, B. 2005. Peatlands of Canada Database. Research Branch, Agriculture and Agri-Food Canada, Ottawa, Ontario, Canada.

Tolson, B. A., and Shoemaker, C. A. 2007. Dynamically dimensioned search algorithm for computationally efficient watershed model calibration. Water Resources Research, **43**(1). doi:10.1029/2005WR004723.

Turcotte, R., Fortin, J. P., Rousseau, A. N., Massicotte, S., and Villeneuve, J. P. 2001. Determination of the drainage structure of a watershed using a digital elevation model and a digital river and lake network. Journal of Hydrology, **374**: 225-242. doi:10.1016/S0022-1694(00)00342-5.

Turcotte, R., Fortin, L., Fortin, V., Fortin, J.-P., and Villeneuve, J.-P. 2007. Operational analysis of the spatial distribution and the temporal evolution of the snowpack water equivalent in southern Quebec, Canada. Nordic Hydrology, **38**: 211-234. doi:10.2166/nh.2007.009.

Turcotte, R., Rousseau, A., Fortin, J.-P., and Villeneuve, J.-P. 2003. A process-oriented, multiple-objective calibration strategy accounting for model structure. *In* Calibration of Watershed Models. *Edited by* Q. Duan, H. Gupta, S. Sooroshian, A. Rousseau, and R. Turcotte. American Geophysical Union, Washington, DC.

Vázquez, R., and Feyen, J. 2003. Effect of potential evapotranspiration estimates on effective parameters and performance of the MIKE SHE-code applied to a medium-size catchment. Journal of Hydrology, **270**: 309-327. doi:10.1016/S0022-1694(02)00308-6.

Verry, E. 1988. Hydrology of wetlands and man's influence on it. *In* Proceedings of the international symposium on the hydrology of wetlands in temperate and cold regions, vol. 2, Joensuu, Finland.

Wang, K., and Dickinson, R. E. 2012. A review of global terrestrial evapotranspiration: Observation, modeling, climatology, and climatic variability. Reviews of Geophysics, **50**(2). doi:10.1029/2011RG000373.

Watt, W. E., and Chow, K. C. A. 1985. A general expression for basin lag time. Canadian Journal of Civil Engineering, **12**: 294-300. doi:10.1139/l85-031.

Wu, J., Kutzbach, L., Jager, D., Wille, C., and Wilmking, M. 2010. Evapotranspiration dynamics in a boreal peatland and its impact on the water and energy balance. Journal of Geophysical Research, **115**(G4). doi:10.1029/2009JG001075.

1060 # Tables

1061 Table 1: Literature review of the impacts of ET_a or ET_p formulations in hydrological modeling.

Reference	Location(s) (Number of sites)	Area [km^2]	Variations in ET	Impacts on hydrological modeling performances
Parmele (1972)	Pennsylvania, U.S.A. (5,) North Carolina, U.S.A. (4)	8-534	Random and systematic errors	Bias has an impact, but not random fluctuations
Andersson (1992)	Sweden (3)	4216-8484	7 different ET_p models	Similar performances
Paturel et al. (1995)	Ivory Coast (5)	368-4700	Systematic errors in ET_p an P	Smaller error with ET_p than with P
Nandakumar and Mein (1997)	Victoria, Australia (22)	0.02-5.2	Systematic error in ET_p and P	Smaller error with ET_p than with P
Joukainen (2000)	Finland (1)	14000	Added parameters to convert ET_p to ET_a	Similar performances
Kokkonen and Jakeman (2001)	North Carolina, U.S.A. (1), Western Australia (1)	0.5-0.8	Different conversion from ET_p to ET_a	Similar performances
Fowler (2002)	Auckland, New Zealand (1)	N/A	Actual ET_p vs. long-term average ET_p	Similar performances
Vázquez and Feyen (2003)	Belgium (1)	586	3 different ET_p models	Strong performance differences
Andréassian et al. (2004)	Massif Central, France (62)	5-89	Improved areal ET_p representation	Similar performances
Oudin et al. (2005)	Australia (8), U.S.A. (79), France (221)	5-9387	Interannual mean ET_p vs. temporally varying ET_p	Similar performances
This study	Québec, Canada (1)	0.97	ET_a measurements vs. 3 ET_p models	Similar performances

Table 2: Review of α scale factors (taken as ET_a / ET_p) for the Penman and Priestley-Taylor models for various peatlands.

	Penman model	
Reference	Study site	α
Koerselman and Beltman (1988)	Quaking fens (The Netherlands)	0.77
Lafleur and Roulet (1992)	Hudson Bay Lowland fens (Canada)	0.75
Campbell and Williamson (1997)	Raised peat bog (New Zealand)	0.34-0.77
Kellner (2001)	Stormossen mire bog (Sweden)	0.61-0.77
Lafleur et al. (2005)	Mer Bleue bog (Canada)	0.44-0.59
Humphreys et al. (2006)	West-East range of peatlands (Canada)	0.38-0.64
Wu et al. (2010)	Salmisuo mire, fen and bog (Finland)	0.59-0.69
	Average α_{lit} used in this study	0.63
	Priestley-Taylor model	
Reference	Study site	α
Kellner (2001)	Stormossen mire bog (Sweden)	0.71-0.85
Petrone et al. (2004)	Bois-des-Bel restored peatland (Canada)	0.67-0.87
Admiral et al. (2006)	Mer Bleue bog (Canada)	0.50-1.50
Humphreys et al. (2006)	West-East range of peatlands (Canada)	0.82-1.05
Petrone et al. (2007)	Wetland-Pond complex (Canada)	0.69
Parmentier et al. (2009)	Horstermeer Polder peatland (The Netherlands)	0.75
Sonnentag et al. (2010)	Sandhill fen (Canada)	0.79-1.04
Brümmer et al. (2012)	Western Peatland and Mer Bleue bog (Canada)	0.60-0.80
Runkle et al. (2014)	Ust-Pojeg mire complex raised bog (Russia)	0.97-1.06
	Average α_{lit} used in this study	0.84

Table 3: Values of α scale factors (ET_a / ET_p) used for each model.

Daily scale		
Model	α_{opt}	α_{lit}
Penman	0.56	0.63
Priestley-Taylor	0.84	0.84
Hydro-Québec	0.76	0.75
Hourly scale		
Model	α_{opt}	α_{lit}
Penman	0.49	0.63
Priestley-Taylor	0.69	0.84
Hydro-Québec	0.69	0.75

Table 4: Performance metrics between observed and modeled ET_a values with α_{opt} and α_{lit}.

Daily scale (α_{opt} ; α_{lit})				
Model	R^2	RMSE [mm]	MB [mm]	NSE
Penman	0.76	0.54 ; 0.62	-0.10 ; 0.17	0.70 ; 0.61
Priestley-Taylor	0.90	0.50 ; 0.50	-0.20 ; -0.19	0.74 ; 0.74
Hydro-Québec	0.62	0.82 ; 0.82	-0.28 ; -0.30	0.32 ; 0.32
Hourly scale (α_{opt} ; α_{lit})				
Model	R^2	RMSE [mm]	MB [mm]	NSE
Penman	0.82	0.048 ; 0.062	-0.017 ; 0.007	0.78 ; 0.64
Priestley-Taylor	0.87	0.047 ; 0.056	-0.025 ; -0.007	0.79 ; 0.71
Hydro-Québec	0.69	0.063 ; 0.064	-0.019 ; -0.013	0.63 ; 0.62

Table 5: Performance metrics between observed and modeled streamflow when using various ET_p observations and models.

Daily scale					
Static sensitivity analysis			Dynamic sensitivity analysis		
Model	RMSE [mm]	NSE	Model	RMSE [mm]	NSE
Observed	0.32	0.89	Observed	0.32	0.89
Penman	0.37	0.85	Penman	0.34	0.87
Priestley-Taylor	0.51	0.72	Priestley-Taylor	0.32	0.89
Hydro-Québec	0.48	0.75	Hydro-Québec	0.32	0.89
Hourly scale					
Static sensitivity analysis			Dynamic sensitivity analysis		
Model	RMSE [mm]	NSE	Model	RMSE [mm]	NSE
Observed	0.015	0.87	Observed	0.015	0.87
Penman	0.017	0.84	Penman	0.016	0.86
Priestley-Taylor	0.022	0.73	Priestley-Taylor	0.015	0.88
Hydro-Québec	0.021	0.75	Hydro-Québec	0.015	0.87

Table 6: Performance metrics difference between observed and modeled streamflow when using various ET_p models.

Daily scale					
Static sensitivity analysis			Dynamic sensitivity analysis		
Model	RMSERD [%]	r^2 [%]	Model	RMSERD [%]	r^2 [%]
Penman	-13.89	**-31.21**	Penman	-5.56	**-15.16**
Priestley-Taylor	-58.33	**-150.31**	Priestley-Taylor	0.00	1.17
Hydro-Québec	-50.00	**-123.68**	Hydro-Québec	0.00	-2.60
Hourly scale					
Static sensitivity analysis			Dynamic sensitivity analysis		
Model	RMSERD [%]	r^2 [%]	Model	RMSERD [%]	r^2 [%]
Penman	-12.20	**-24.96**	Penman	-4.88	-9.43
Priestley-Taylor	-46.34	**-117.27**	Priestley-Taylor	2.44	2.93
Hydro-Québec	-39.02	**-98.57**	Hydro-Québec	0.00	-0.24

Figures

Figure 1: (a) Satellite image of the watershed (adapted from Google Earth, 2017) with instruments location; (b) Topographical map of the watershed with instruments location; (c) Flux tower at the site (20 July 2012); (d) Trapezoidal flume at the outlet (adapted from Clerc, 2009).

Figure 2: Seasonal variation of each fluxes of the water budget at the Necopastic peatland watershed. Air temperature T_a is shown on the first plot (precipitation P) and water table depth WTD is shown on the 4th plot (groundwater storage change S).

Figure 3: Seasonal variation of cumulative fluxes of water at the Necopastic peatland watershed.

Figure 4: Comparison between modeled and observed ET_a for: (a) daily and (b) hourly scales. The first column is Penman; the second, Priestley-Taylor, and the third, Hydro-Québec. The first row of each timescale uses α_{opt} for model computation, while the second row uses α_{lit}. The solid lines are least squared regressions of the data with statistics shown on the graphs, while the dashed lines are 1:1 lines. Potential outliers are shown with a cross (“x”).

Figure 5: Time series of cumulative $ET_{a,EC}$ and modeled ET_a using: a) α_{opt} (daily time steps); b) α_{lit} (daily time steps); c) α_{opt} (hourly time steps); and d) α_{lit} (hourly time steps). The dashed line is the total cumulative evaporated water from observations $ET_{a,EC}$ (224 mm).

Figure 6: Hydrographs of observed and modeled streamflow. The latter are those obtained when using $ET_{p,EC}$ (black dashed) and every version of modeled ET_p (Penman: blue; Priestley-Taylor: red; Hydro-Québec: grey), during either static (dashed lines) and dynamic (full lines) analysis. Precipitation is shown on top histogram.

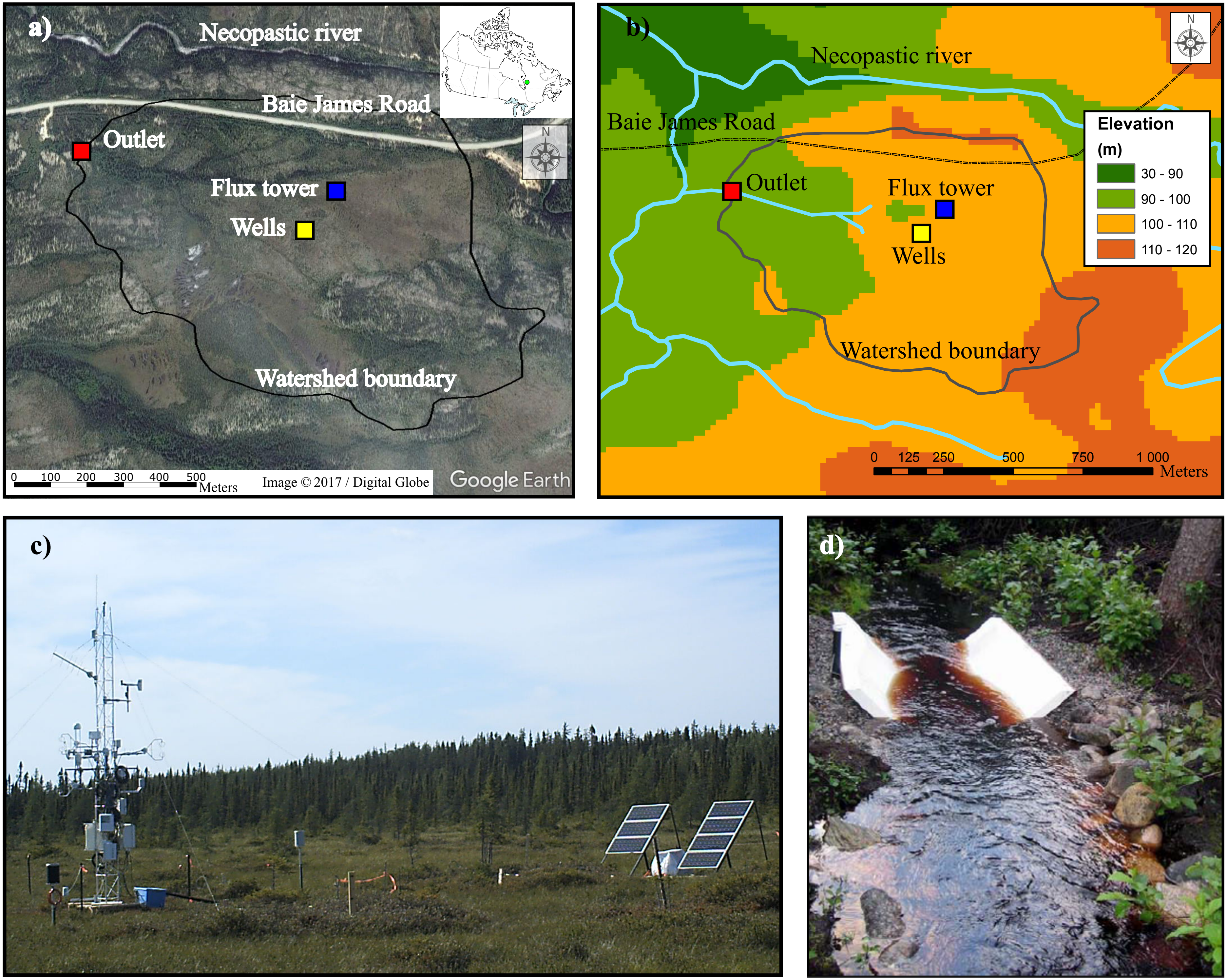
a)
Necopastic river
Baie James Road
Outlet
Flux tower
Wells
Watershed boundary
N
0 100 200 300 400 500
Meters
Image © 2017 / Digital Globe
Google Earth
b)
Necopastic river
Baie James Road
Outlet
Flux tower
Wells
Watershed boundary
N
Elevation (m)
30 - 90
90 - 100
100 - 110
110 - 120
0 125 250 500 750 1 000
Meters
c)
d)

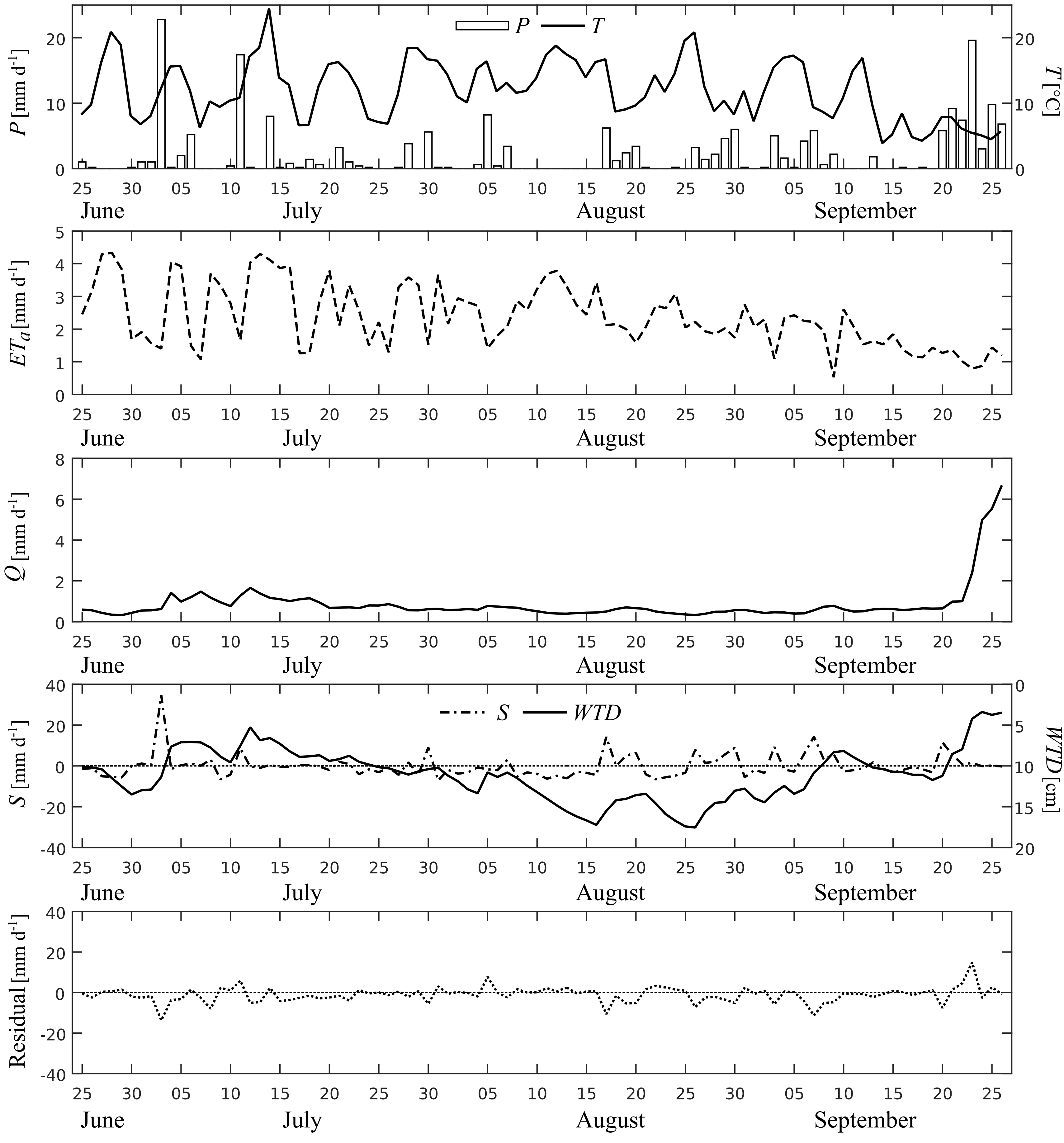
P
T
P [mm d-1]
T [°C]
ETa [mm d-1]
Q [mm d-1]
S
WTD
S [mm d-1]
WTD [cm]
Residual [mm d-1]
25 30 05 10 15 20 25 30 05 10 15 20 25 30 05 10 15 20 25
June
July
August
September

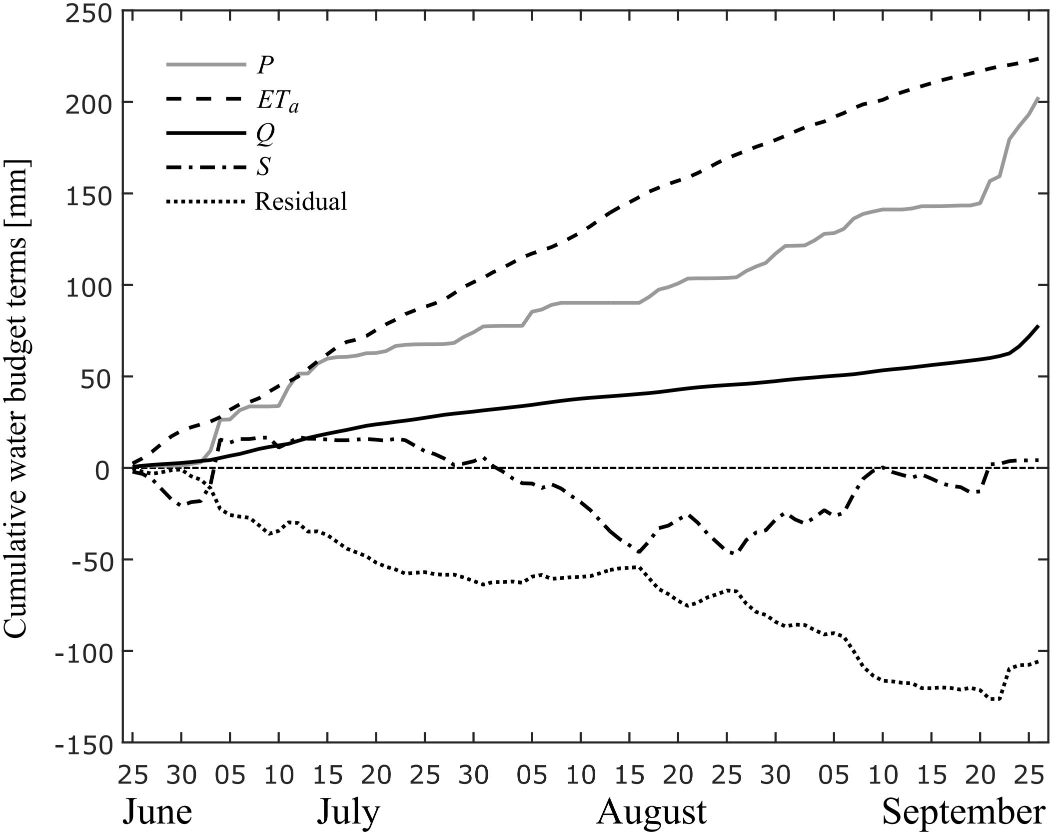
P
ETa
Q
S
Residual
Cumulative water budget terms [mm]
250
200
150
100
50
0
-50
-100
-150
25 30 05 10 15 20 25 30 05 10 15 20 25 30 05 10 15 20 25
June
July
August
September

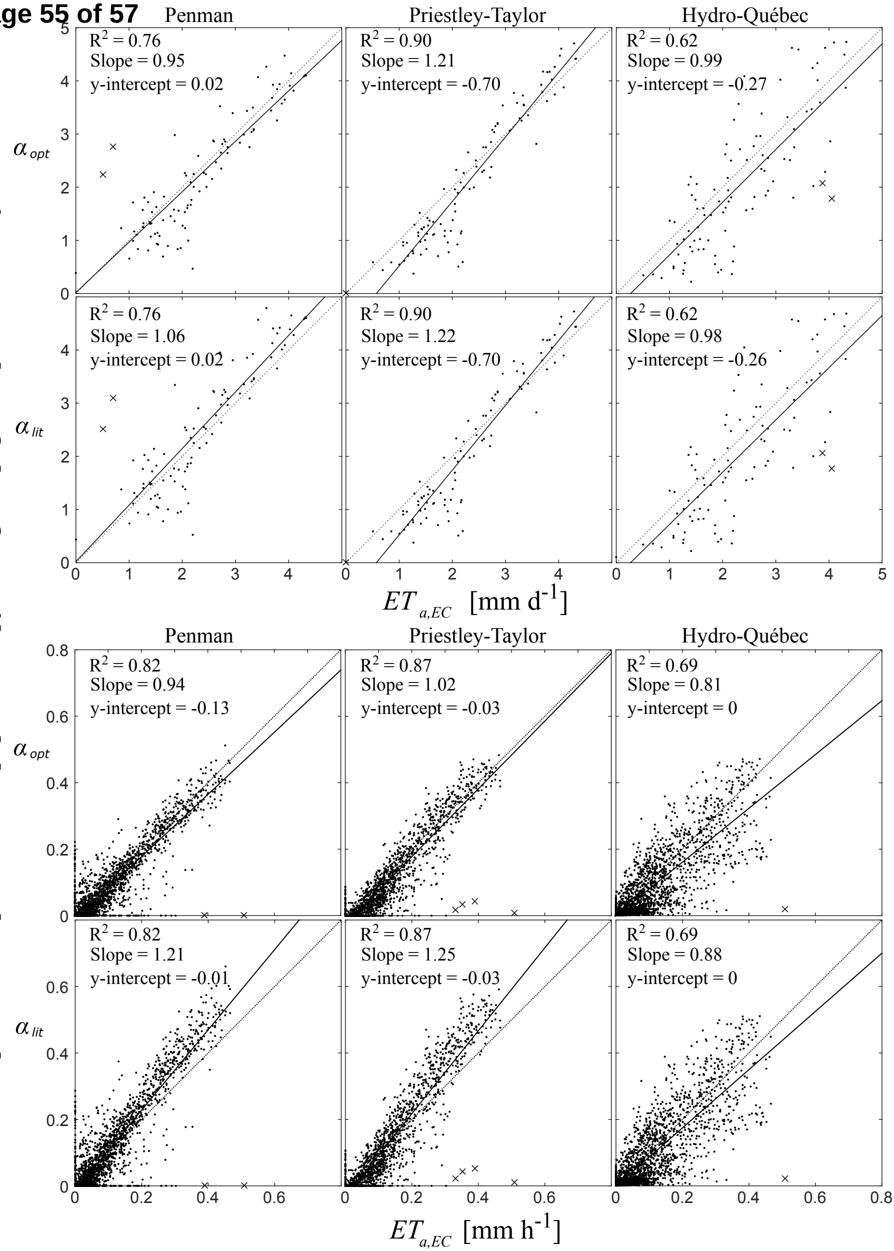
a
Penman
Priestley-Taylor
Hydro-Québec
R² = 0.76
Slope = 0.95
y-intercept = 0.02
R² = 0.90
Slope = 1.21
y-intercept = -0.70
R² = 0.62
Slope = 0.99
y-intercept = -0.27
R² = 0.76
Slope = 1.06
y-intercept = 0.02
R² = 0.90
Slope = 1.22
y-intercept = -0.70
R² = 0.62
Slope = 0.98
y-intercept = -0.26
α opt
α lit
Modeled ET a [mm d-1]
ET a,EC [mm d-1]
b
Penman
Priestley-Taylor
Hydro-Québec
R² = 0.82
Slope = 0.94
y-intercept = -0.13
R² = 0.87
Slope = 1.02
y-intercept = -0.03
R² = 0.69
Slope = 0.81
y-intercept = 0
R² = 0.82
Slope = 1.21
y-intercept = -0.01
R² = 0.87
Slope = 1.25
y-intercept = -0.03
R² = 0.69
Slope = 0.88
y-intercept = 0
Modeled ET a [mm h-1]
ET a,EC [mm h-1]

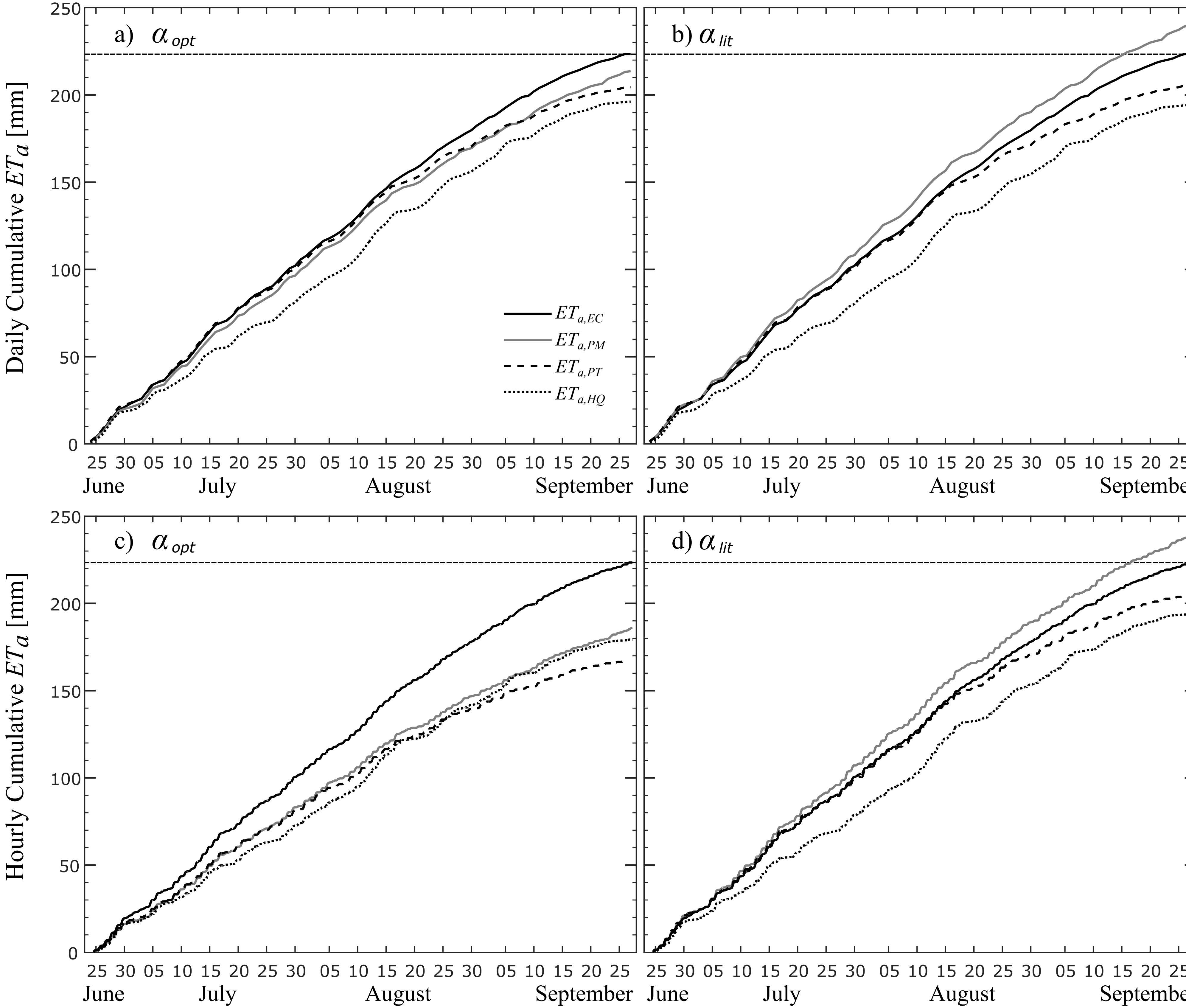
a) α_{opt}
b) α_{lit}
c) α_{opt}
d) α_{lit}
Daily Cumulative ET_a [mm]
Hourly Cumulative ET_a [mm]
$ET_{a,EC}$
$ET_{a,PM}$
$ET_{a,PT}$
$ET_{a,HQ}$
0
50
100
150
200
250
25 30 05 10 15 20 25 30 05 10 15 20 25 30 05 10 15 20 25
June
July
August
September

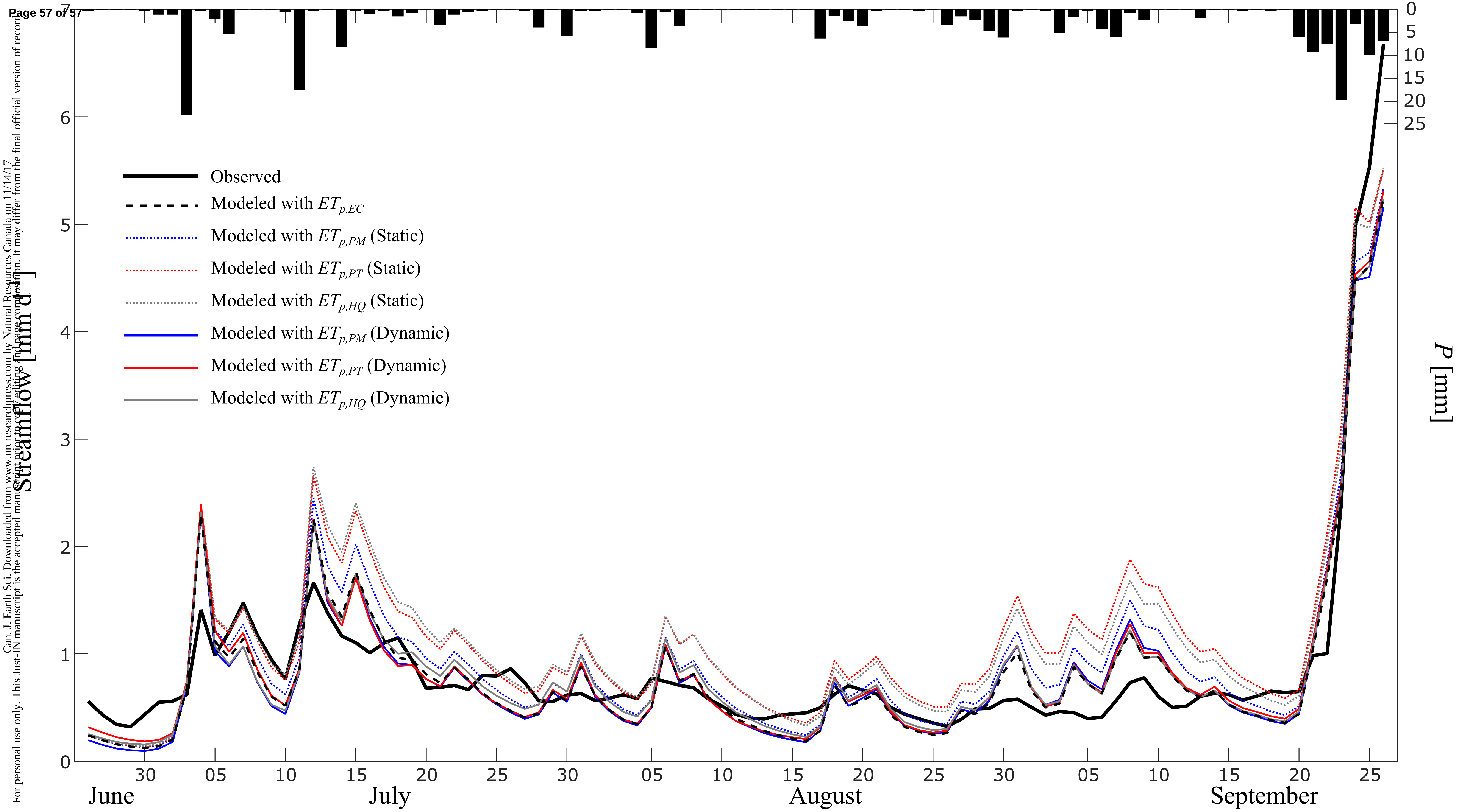
Streamflow [mm d⁻¹]
P [mm]
Observed
Modeled with $ET_{p,EC}$
Modeled with $ET_{p,PM}$ (Static)
Modeled with $ET_{p,PT}$ (Static)
Modeled with $ET_{p,HQ}$ (Static)
Modeled with $ET_{p,PM}$ (Dynamic)
Modeled with $ET_{p,PT}$ (Dynamic)
Modeled with $ET_{p,HQ}$ (Dynamic)
June
July
August
September